The Pennsylvania State University

The Graduate School

Department of Electrical Engineering

CHARACTERIZATION OF LOW-LEVEL JETS AND THEIR INFLUENCE ON AIR POLLUTION USING RAMAN LIDAR AND WIND PROFILING RADAR/RASS

A Thesis in

Electrical Engineering

by

Sachin John Verghese

Submitted in Partial Fulfillment
of the Requirements
for the Degree of

Master of Science

August 2003

_____

Sachin John Verghese

The thesis of Sachin John Verghese has been reviewed and approved* by the following:

C. Russell Philbrick
Professor of Electrical Engineering
Thesis Adviser

Lynn Carpenter
Associate Professor of Electrical Engineering

R. D. Clark
Professor of Meteorology
(Millersville University)

Kenneth Jenkins
Professor of Electrical Engineering
Head of the Department of Electrical Engineering

*Signatures are on file in the Graduate School.

ABSTRACT

Raman lidar employed simultaneously with wind measurements of a radar/RASS (Radio Acoustic Sounding System) profiler are used to characterize features of nocturnal jets or Low-Level Jets (LLJ's) and the effect they have on the local meteorology. While the radar/RASS measurements document the kinematic and thermodynamic structure by identifying the velocity and virtual temperature distributions, the PSU Lidar Atmospheric Profile Sensor (LAPS) observations provide high temporal and spatial resolution of the water vapor mixing ratio, temperature, ozone concentration, and optical extinction. Data was obtained from the two instruments during the NARSTO-NE-OPS (North American Research Strategy for Tropospheric Ozone – North East – Oxidant and Particle Study) case studies, which was conducted in the Philadelphia urban environment during the summers of 1999, 2001 and 2002. The PSU LAPS instrument uses Raman scattering techniques to provide vertical profiles of the atmospheric properties. The wind profiling radar is a pulsed Doppler radar and provides continuous profiles of the wind characteristics. The PSU Raman lidar and the radar/RASS profiler are used to delineate the physical characteristics of the LLJ, its development, evolution and the variations in observed parameters associated with the LLJ phenomena. LLJ's have been associated with high ozone events since both LLJ's and high ozone episodes occur under similar meteorological conditions. An important finding is the intrusion of drier air with ozone and precursor concentrations as the LLJ become a conveyor of air from the western boundary region during the early hours of the morning. This transport reservoir increases the concentrations of pollutants drastically when it is mixed down to the surface by

convective heating and by bursting events. Analysis of the data revealed that low-level jets were present on 7 out of 8 nights prior to days when ozone concentrations exceeded 100 ppbv. The results obtained clearly indicate the low-level jet to be an important mechanism in the generation of pollution episodes due to its capability to transport pollutant and precursor materials over long distances during the night and produce high concentrations of pollutants the following day.

TABLE OF CONTENTS

LIST OF FIGURES

LIST OF TABLES

ACKNOWLEDGMENTS

I would like to thank all those who contributed to this work. Primarily, sincere appreciation is extended to my thesis advisor, Dr. C. R. Philbrick, for his professional guidance and patience. I would also like to thank him for giving me the opportunity to work in his lab and for teaching me valuable lessons in research and in life.

I would like to thank Dr. Richard Clark, Dr. Lynn Carpenter, and William. F. Ryan for their advice and guidance. Thanks are due to Adam Willitsford, Homer Li, Jason Collier, Sameer Unni and Sriram Kizhakemaddem for their encouragement and friendship.

Throughout my life my family has been very supportive. I would like to thank my parents and brother for believing in me and for always being there for me when I needed them. Special thanks are due to my best friend, Divya, for her constant encouragement and inspiration.

I acknowledge the support of my graduate research by the United States Environmental Protection Agency, grant # R826373, and by the Pennsylvania Department of Environmental Protection.

CHAPTER 1

INTRODUCTION

Nocturnal jets, or Low-Level Jets (LLJ's), are recurring features of the mid-Atlantic region under conditions of weak synoptic forcing. The influence of LLJ's on the local and regional meteorology can be dramatic because they can transport pollutants and precursor materials hundreds of kilometers, during the night, without generating much of a signal at the surface. As the boundary layer develops the following morning, higher pollutant concentrations aloft, that are often double the background values, are mixed down to the surface. These pollutants and precursor materials may produce a rapid increase in pollutant concentrations that are more significant than can be generated by local urban primary and secondary pollutant productions. These transported precursors can result in high ozone concentrations and can also result in aerosol haze formation. A strong correlation is found between the occurrence of LLJ's and high ozone episodes. My hypothesis is that LLJ's contribute to air pollution episodes in Philadelphia and along the northeast corridor. This problem requires investigation of the relationship that exists between the presence of LLJ's and pollution episodes, and determination of whether LLJ's play a vital role in the generation of high ozone episodes along the northeast corridor.

Over the past few decades, human activity, particularly industrial activity, power generation and automobile exhaust have been shown to be the major air pollution sources. Our atmosphere is contaminated as a consequence, and hence, the air we breathe affects our health and influences our daily activities. Meteorological processes have been

seen to have a profound controlling effect on pollution [Arya, 1999]. Weather influences pollution in a number of ways that can both concentrate and dissipate the pollution, such as transport of pollution by winds from one place to another, stagnation of an air mass, dilution of the pollutants, and rainout effects. These influences are important because the local surface concentrations of pollutants are not only due to their formation through photochemical reactions, but also due to processes that control their transport, residence times, and control the transport of precursor materials from outside regions. Ozone and airborne particulate matter (PM) are the two principal components of the atmosphere that have been singled out as major concerns of air pollution. Our knowledge on the atmosphere has greatly improved during the last several years due to the emphasis on investigations using sophisticated optical remote sensing techniques. An improved understanding of the influence of local and regional transport on sources, sinks, mixing, and a better understanding of photochemical transformations that control the abundances of oxidants and fine particles are keys to developing any capability for future forecasting of such pollution events and lessening their harmful effects.

Measurements obtained from the NE-OPS (North-East Oxidant and Particle Study) campaigns in Philadelphia during the summers of 1999, 2001 and 2002 have been analyzed to investigate the influence that nocturnal jets (LLJ's) have on modifying the properties of the residual boundary layer. The primary objectives of the NE-OPS campaigns are to investigate the urban polluted atmosphere to find the relationships among conditions that lead to high ozone concentrations and increased levels of fine particles, determine the contributions from local and distant sources, and examine the role that meteorological properties play in the build-up and dissipation of pollutant

concentrations. The two primary instruments that are used to characterize LLJ's and their effects are the PSU Lidar Atmospheric Profile Sensor (LAPS) and a wind profiling radar/RASS. The LAPS system uses Raman scattering techniques to measure vertical profiles of ozone, water vapor, temperature, and aerosol extinction. The profiles are obtained each minute, with a vertical resolution of 75 meters and the lidar has the capability of operating continuously during daytime and nighttime. The wind profiling radar is a pulsed Doppler radar and uses refractive irregularities and particulates in the atmosphere as scattering targets. The Radio Acoustic Sounding System (RASS) provides profiles of virtual temperature from measurements of the speed of sound using vertically directed acoustic waves observed by the radar profiler. It is particularly interesting that signatures of LLJ's have been identified in the Millersville University's surface trace gas analyzers, and Clarkson University's Aethalometer and OC/EC instruments, which were also used during the NE-OPS campaigns. During the NE-OPS campaigns, LLJ's were observed on several nights by the wind profiling radar and the influence that these events have on the local meteorology is clearly seen in the data obtained from the Raman lidar and the other instruments.

Hence, this thesis uses the large database obtained during the NE-OPS campaigns to investigate and understand the correlations that are seen to exist between LLJ's and air-pollution episodes. The data will help explain the effects that these jets have on modifying the properties of the residual layer and the role that they play in the development of high ozone episodes. The instrument operation and data collection techniques used in these studies, primarily the PSU LAPS system and the wind profiling radar/RASS, are described. Measurements from other sites, such as the Rutgers

University, NJ and Fort Meade, MD profilers, have been used to characterize certain features of these nocturnal jets, such as horizontal extent and characteristic height. The data obtained from the three profilers along the northeast corridor will help in defining certain criterion for identifying LLJ's that are observed along the east coast region. Back trajectories from NOAA (http://www.arl.noaa.gov/ready.html) indicate the regions from which nocturnal jets transport the pollutant and precursor materials, and this will help us in identifying the specific pollutants that are being advected along by the nocturnal jets.

CHAPTER 2

INSTRUMENTATION AND MEASUREMENT TECHNIQUES

2.1 Introduction

Remote sensing instruments help us to observe and continuously monitor the Earth's surface and atmosphere on a global scale. They have greatly improved our understanding of the world and the functioning of its environment. A combination of remote sensing instruments, Raman lidar and wind profiling radar/RASS, were used to study low-level jets over Philadelphia during the NE-OPS case studies of 1999, 2001 and 2002. During these summers the wind profiler observed several low-level jets, while their characteristic signatures were seen in the water vapor and ozone profiles measured by the PSU Raman lidar. This chapter briefly describes the theory of operation and measurement techniques of Penn State's LAPS Raman lidar and the wind profiling Radar/RASS.

2.2 Lidar Atmospheric Profile Sensor (LAPS) Lidar

The Lidar Atmospheric Profile Sensor (LAPS) instrument was built by the staff and graduate students of the Applied Research Laboratory and the College of Engineering of Penn State University for the U.S Navy as an operational prototype. The LAPS Raman lidar provides the profiles of water vapor and temperature as real time data products to support requirements for profiles of RF-refraction and meteorological data [Philbrick, 1998]. The LAPS instrument uses Raman lidar techniques to simultaneously provide profiles of water vapor, temperature, ozone and optical extinction [Philbrick,

2001]. These measurements provide the key results for understanding the processes involved in the evolution of pollution episodes. LIDAR is the acronym for LIght Detection and Ranging. The LAPS laser transmitter sends a pulsed beam at the doubled (532 nm) and quadrupled (266 nm) wavelength of the Nd:YAG laser into the atmosphere and a telescope receives the signals that have been scattered by the molecules and particles of the atmosphere. The time interval between the transmission of the pulse and the reception of its backscatter signal gives the altitude of the scattering volume. Measurements of the atmospheric constituents are obtained from the return signal intensity at the transmitted wavelength as well as at Raman shifted wavelengths. LAPS was first tested onboard a U.S. Navy ship, the USNS SUMNER during September and October 1996 in the Gulf of Mexico and Atlantic Ocean. Since then it has been used in a number of research investigations, which have been mainly concerned with understanding air pollution episodes. PSU's LAPS is a rugged instrument and was designed for automatic operation to enable measuring in virtually any environment at any given time. Raman lidar measurements of atmospheric properties are expected to provide a large contribution to the meteorological data in the future.

Penn State University's LAPS lidar consists of more than twenty sub-systems to control its operation and obtain measurements. The main components of the LAPS system are the transmitter, receiver, detector, data collection electronics, and control system. The transmitter, receiver and control system are housed in a weather sealed unit so that it can be deployed in an outdoor environment and operated under a wide range of conditions. The unit includes an environmental sub-system, with air-conditioner and heater, to maintain the instrument at its acceptable operating temperature. This primary

part of the instrument has been termed as the 'Deck Unit'. The deck unit also includes a safety radar system to automatically shut down the laser beam when an aircraft approaches a 6º cone angle around the beam. Another system called the 'Console Unit' houses the command computer, detector, and the data analysis and display electronics. The console unit and the deck unit are connected by power lines and fiber optic cables, which are used to control the system operation and to transfer the received signals from the receiver telescope to the detectors. The primary subsystems of LAPS are summarized in Table 2.1.

Table 2.1 Summary of LAPS subsystems [Mulik, 2000].

Transmitter	Continuum 9030 –30 Hz 5X Beam Expander	600 mJ @ 532 nm 130 mJ @ 266 nm
Receiver	61 cm Diameter Telescope Focal length – 1.5 m	Fiber optic transfer
Detector	Eight PMT channels Photon Counting	660 and 607 nm – Water Vapor 528 and 530 nm – Temperature 295 and 284 nm – Daytime Water Vapor 277 and 284 nm – Raman/DIAL Ozone 607, 530, and 284 nm – Extinction 532 nm – Backscatter
Data System	DSP 100 MHz	75-meter range bins
Safety Radar	Marine R-70 X-Band	Protects 6? cone angle around beam

The transmitter is a Nd:YAG laser, which operates at a fundamental wavelength of 1064 nm. The Nd:YAG laser is pulsed at 30 Hz with an output power of 1.6 joules per pulse at 1064 nm. Frequency doubling and quadrupling crystals are used to generate the second harmonic (532 nm) and fourth harmonic (266 nm) from the fundamental wavelength (1064 nm). The residual primary wavelength is then dumped inside the instrument on a water cooled surface by a dichroic beamsplitter, while the 532 nm and 266 nm beams are sent through a 5X beam expander and then into the atmosphere. It has

been proposed to use the 355 nm transmission wavelength in the design of the Advanced LAPS (ALAPS) system [Slick, 2002]. The laser transmitter system of LAPS is shown in Figure 2.1. Characteristics of the transmitter section are given in Table 2.2.

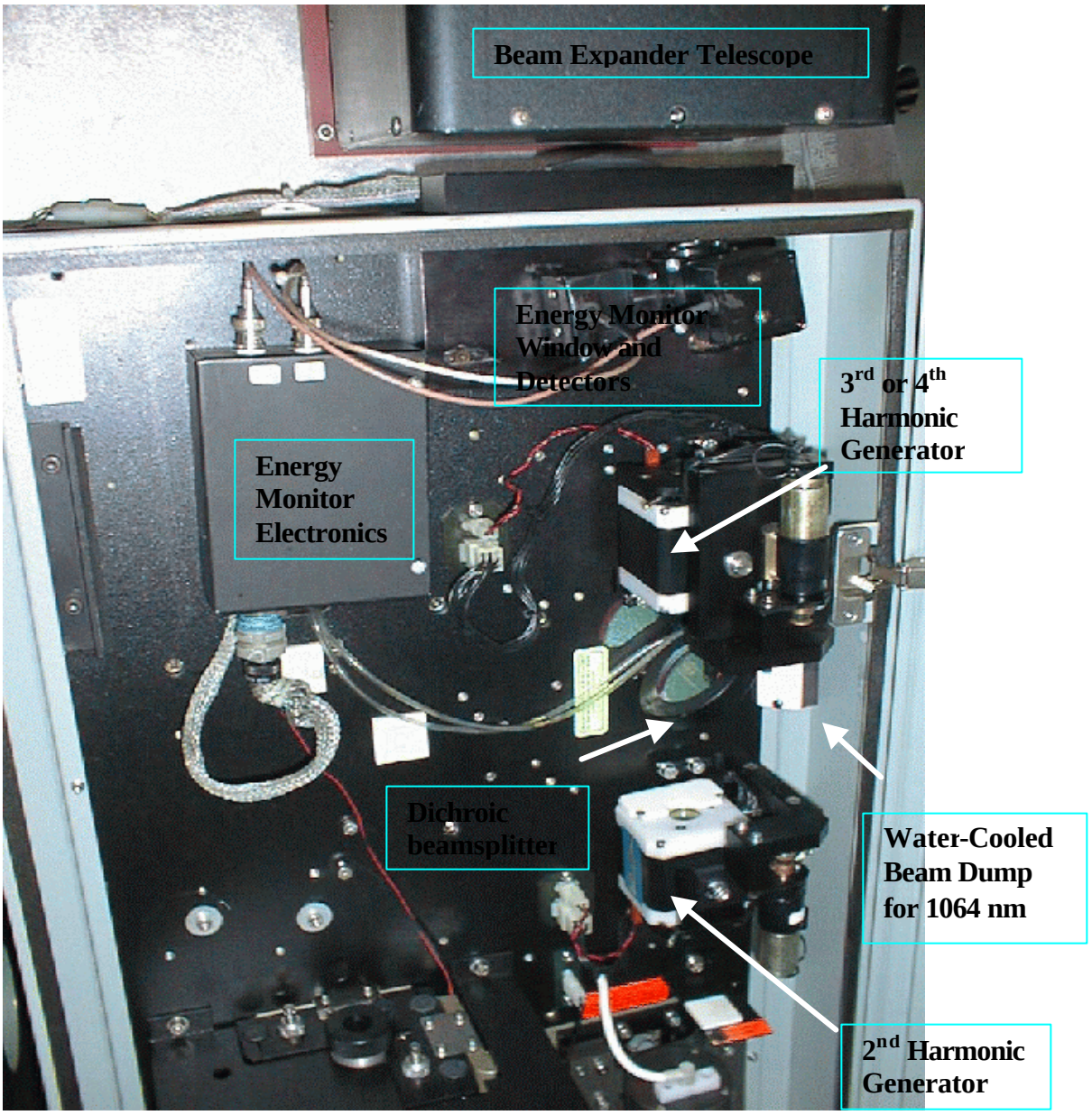

Figure 2.1 LAPS Transmitter optics (photo credit, C.R. Philbrick).

Table 2.2 LAPS transmitter characteristics [Philbrick, 1998].

Laser	Continuum Model 9030 with 5X Beam Expander
Pulse Repetition Frequency	30 Hz
Pulse Duration	8 ns
Fundamental Power	1.6 J/Pulse
Power Output at 1064 nm	Dumped into heat sink
Power Output at 532 nm	600 mJ
Power Output at 266 nm	120 mJ

The 5X beam expander is used to expand the beam from 9 mm diameter to 4.5 cm diameter. The larger cross-section area achieved with the beam expander serves two purposes by ensuring a power density below ANSI standards for near-field diffuse reflections and by reducing the beam divergence for a smaller field-of-view at a distance. The beam expander decreases the divergence of the transmitted beam by five times to about 80 ?rad so that it is well contained within the 250 µrad field of view of the telescope and fiber combination [Slick, 2002]. The deck unit also consists of a X-band radar, which is used to prevent any hazard due to reflection from an aircraft flying through the beam. The radar forms a 6° protecting cone around the beam and shuts the beam off automatically if it detects an intrusion. It is designed to automatically disable the laser Q-switch if a targets return signal is detected. The radar operates at 9375 MHz with a peak pulse power of 10 kW.

Since a lidar receiver is a light collecting system and not an imaging system, the two main requirements of the receiver are to collect light backscattered from a minimum near-field distance to infinity, and to concentrate the collected light inside a field stop aperture or optical fiber [Jenness et al, 1997]. The receiver subsystem, shown in Figure 2.2, consists of a reflecting telescope, constructed with a parabolic mirror 61 cm in diameter with a focal length of 1.5 m, and a fiber optic cable. The fiber optic cable is 1

mm in diameter and is located at the focal point of the mirror. The position of the fiber can be easily adjusted from the console by computer-controlled 3-axis micropositioners. The return signal is reflected and focused into a 1mm fiber as shown in Figure 2.2. Fiber

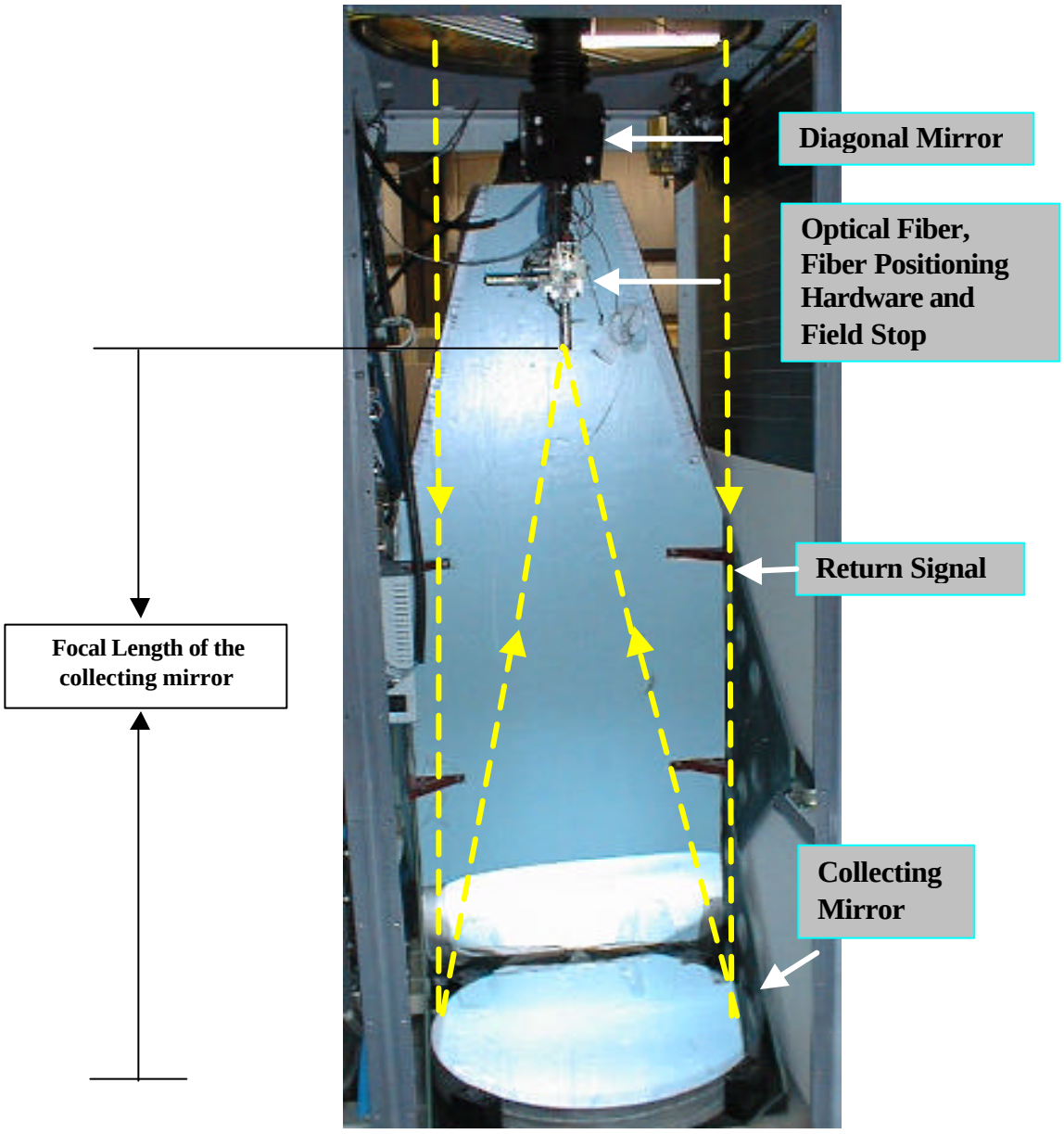

Figure 2.2 Receiver components and schematic of received beam (photo credit, C.R. Philbrick).

optic cables are convenient for transfer of return light to the remote detector box and they also serve as a field stop to limit the transfer of background light to the detector box [Jenness et al, 1997]. The fiber optic cables transfer the return signal to the detector box in the console unit, where the Raman wavelengths are separated and the signal photons are converted to digital pulses by the photomultiplier tubes (PMT's), which are used in pulse detection mode. In the detector box, seven of the filters are selected at the vibrational and rotational Raman-shifted wavelengths corresponding to the laser wavelengths at 532 nm and 266 nm. The eighth filter is centered at 532 nm to measure direct backscatter. The light entering into the detector box from the fiber optic cable is then directed towards each of the filters using wavelength-separating (dichroic) and intensity-separating beamsplitters.

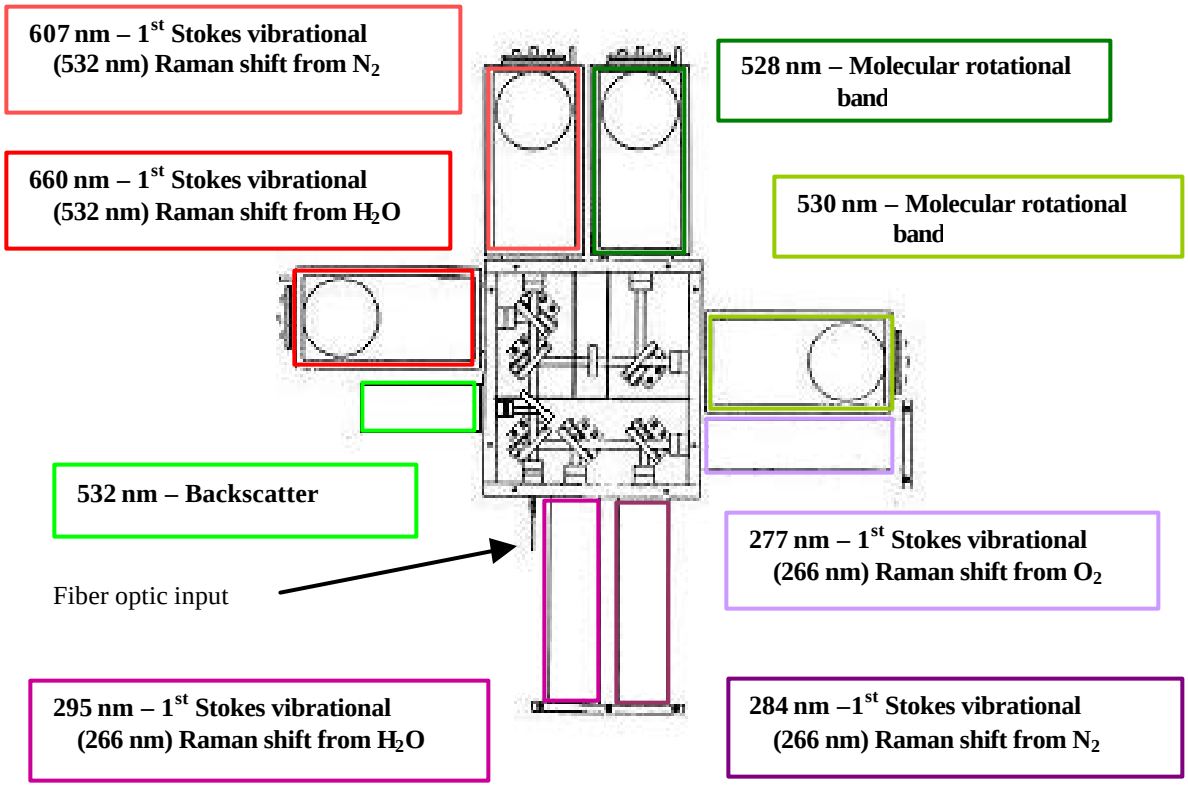

Figure 2.3 LAPS detector box with steering optics and the layout of each PMT

The signals pass through their respective narrowband filters and are then transferred to photon counting PMT's. High sensitivity PMT's are used because the Raman scattered signals are weak due to small scattering cross-sections. For optimal detection performance of the Raman signals, the PMTs should have high collection efficiency, good multiplication statistics, low noise, and high photocathode quantum efficiency in the spectral range of interest. In order to stabilize gain sensitivity, reduce dark current effects, and provide a linear response over a large dynamic range, the PMTs in the LAPS detector are used in the photon counting mode. This means the individually generated current pulses for each photoelectron generated event are counted, rather than performing an A/D conversion on the DC current levels [Chada, 2001]. Data from the seven wavelength channels are stored simultaneously in half-microsecond channels, which provide bins of 75 m resolution.

The console unit consists of the command computer, detector, photon counting electronics, and the data processor. It is possible to control all the subsystems of LAPS from the command/analysis computer in the console unit. When the system is in operation, the data acquisition system transfers the data signals, as photon counts detected by the PMT's, to the computer for processing. The raw data is processed in real time and vertical profiles of atmospheric temperature, water vapor concentration, ozone, and raw photon counts are displayed. LAPS has a vertical resolution of 75 meters for seven of the PMT's and a vertical resolution of 3 meters for the backscatter detector. The raw data is used to profile the water vapor mixing ratio, ozone, temperature and extinction using the lidar equation, which will be discussed in Section 2.2.2.

2.2.1 Raman Scattering

Penn State University's LAPS lidar measures the properties of the atmosphere from the Raman scatter signals generated by the laser beam interaction with the molecules of the atmosphere. Consider the process where electromagnetic energy is scattered by a molecule. The process can be considered as a photon of the incident radiation field being destroyed and a photon of scattered radiation being created. The process is said to be elastic (Rayleigh scattering) if the scattered frequency is nearly the same as the incident frequency and inelastic (Raman scattering) if the scattered frequency and the incident frequency are different. Raman scattering shifts the frequency of the scattered photon by the amount of the energy difference associated with the vibrational and rotational energy states of the scattering molecule. These scattering processes are shown schematically in Figure 2.4. The scattered radiation is seen to have a lower frequency when the molecule gains energy from the radiation field, a process referred to as the Stokes component. The anti-Stokes component or the higher frequency radiation results when the molecule loses energy to the radiation field in the rare case when the molecule resides in an upper vibrational level [Measures, 1984].

The intensity of Stokes vibrational Raman scattering is roughly one-thousandth that of Rayleigh scattered component. The sensitivity of the process is thus usually limited to the detection of molecules occurring in high concentrations. Classification of the various optical interaction processes in laser remote sensing is given in Table 2.3. Raman scattering and fluorescence are the two interaction processes that exhibit inelastic scattering. Fluorescence can be used for high sensitivity detection of molecules, due to its large emission cross section. In the lower atmosphere, however, fluorescence intensity is

reduced by collision quenching with air molecules depending on pressure, temperature and humidity, and the emission spectrum is spread over many spectral lines in most molecules [Kobayashi, 1987]. These factors limit the application of this process in remote sensing in the lower atmosphere.

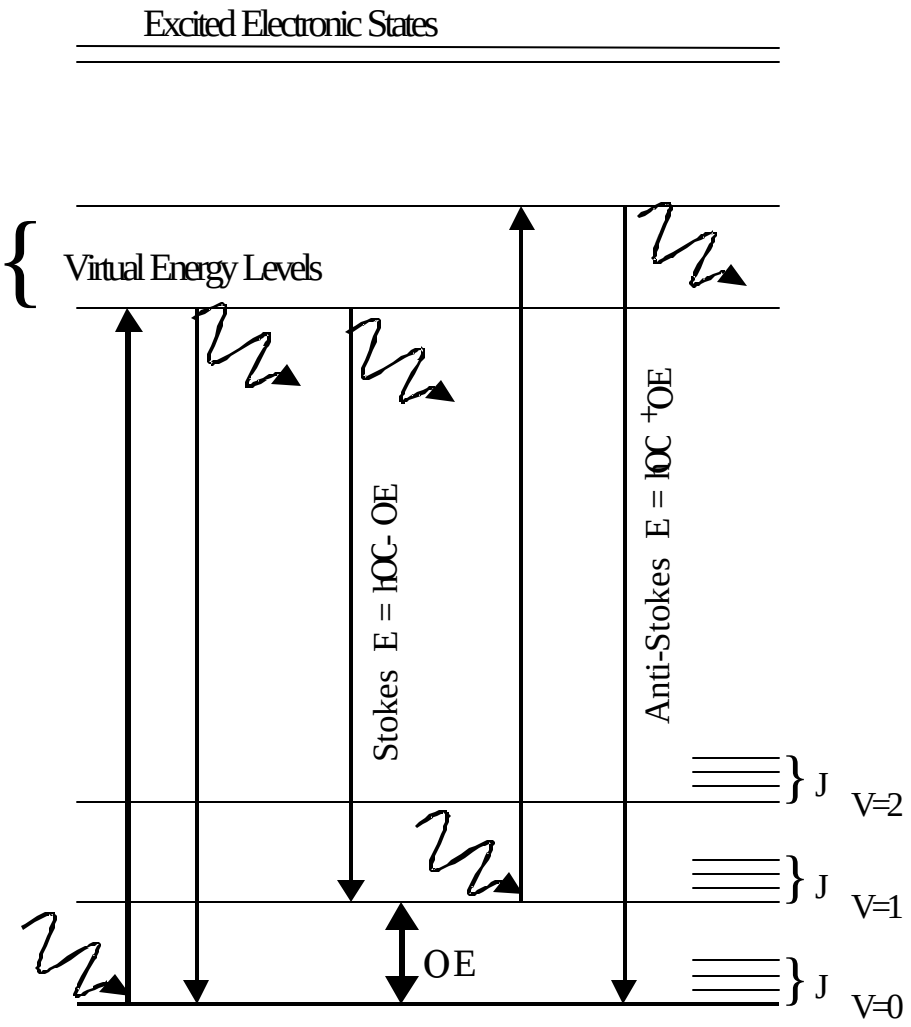

Figure 2.4 Energy diagram representation of the Stokes and anti-Stokes components due to Raman scattering [Philbrick, 1994].

Table 2.3 Optical interaction processes used in laser remote sensing (Kobayashi, 1987).

Interaction process	Received wavelength	Interaction cross section (m^2)	Detectable matter
Mie scattering	$?_0$	$10^{-28} \sim 10^{-10}$	Particle
Rayleigh scattering	$?_0$	$\sim 10^{-29}$	Atom, Molecule
Raman scattering	$?_0 ? ??$	$10^{-35} \sim 10^{-30}$	Molecule
Fluorescence	$?_0 ? ???$	$10^{-29} \sim 10^{-27}$	Atom, Molecule
Resonance scattering	$?_0$	$10^{-18} \sim 10^{-15}$	Atom
Absorption	$?_0$	$10^{-24} \sim 10\text{-}^{15}$	Atom, Molecule

The Raman scattering technique is advantageous because of its quantitative measurement capabilities using a single fixed wavelength. Raman scatter signals can be used to identify a trace constituent and quantify it relative to the major constituents of a mixture [Measures, 1984]. The LAPS instrument uses the vibrational Raman scattered signals to measure water vapor, ozone and optical extinction, and uses the rotational Raman scatter signals to measure temperature. It collects the rotational Raman backscatter signals at 528 nm and 530 nm and the vibrational Raman backscatter signals at 607 nm, 660 nm, 277 nm, 284 nm and 295 nm. The 607 and 660 nm signals are the 1st Stokes vibrational Raman shifts from the N_2 and H_2O molecules in the atmosphere excited by the second harmonic (532 nm) of the Nd:YAG laser. The 277, 284 and 295 nm signals correspond to the 1st Stokes vibrational Raman shifts from the O_2, N_2, and H_2O molecules in the atmosphere excited by the fourth harmonic (266 nm) of the Nd:YAG laser. The ratio of rotational Raman signals at 528 and 530 provides the measurement of atmospheric temperature [Haris, 1995]. Since the rotational states of all

the molecules in the lower atmosphere are distributed according to the local temperature, the temperature can be directly measured by taking the ratio of the backscatter signals at two wavelengths in this distribution. Optical extinction is measured using the gradient of the measured molecular profile compared with that expected for the density gradient [O'Brien et al, 1996]. Techniques to measure water vapor and ozone will be discussed in Sections 2.2.3 and 2.2.4 respectively. The measurement capabilities of the LAPS instrument using Raman scatter techniques are summarized in Table 2.4.

Table 2.4 LAPS measurement capabilities using Raman scatter techniques [Esposito, 1999].

Property	Measurement	Altitude (km)	Time Resolution
Water Vapor	660/607 Raman 295/284 Raman	Surface to 5 Surface to 3	Night - 1 min. Day/Night - 1 min.
Temperature	528/530 Rotational Raman	Surface to 5	Night - 30 min.
Optical Extinction - 530 nm	530 nm Rotational Raman	Surface to 5	Night 10 to 30 min.
Optical Extinction - 607 nm	607 nm Vibrational Raman	Surface to 5	Night 10 to 30 min.
Optical Extinction - 284 nm	284 nm Vibrational Raman	Surface to 3	Day/Night 30 min.
Ozone	277/285 Raman/DIAL	Surface to 2 - 3	Day/Night 30 min.

2.2.2 Lidar Equation

Using the LAPS instrument, profiles of water vapor, ozone and optical extinction are obtained from the vibrational Raman scatter, while rotational Raman scatter signals are used to measure temperature profiles. The raw photon counts obtained from the

backscatter of the laser radiation provides us with information about the concentrations of N_2, O_2, and H_2O at different altitudes. Since LAPS utilizes the backscatter of the laser beam, the form of the lidar equation is fairly simple, but the interpretation of the lidar signal is complicated by geometrical considerations that include the degree of overlap between the laser beam and the field of view of the receiver optics as well as the details of the telescope. The reader can refer to Measures [1984] for the derivation of the scattering lidar equation, which is described by the power of the signal received by a monostatic lidar denoted by $P(?_R,z)$, given by :

$$P(?_R, z) ? P_T(?_T)?_T(?_T)?_R(?_R)\frac{c?}{2}\frac{A}{z^2} ?(?_T, ?_R)\exp\left[-2\int_0^z [? (?_T, z') ? ? (?_R, z')]dz'\right] \qquad [2.1]$$

where,

z	is the altitude of the volume element from which the return signal is scattered [m],
$?_T$	is the wavelength of the laser light transmitted [m],
$?_R$	is the wavelength of the signal received [m],
$P_T(?_T)$	is the power transmitted at wavelength $?_T$ [W],
$?_T(?_T)$	is the net optical efficiency at wavelength $?_T$ of all transmitting elements [unitless],
$?_R(?_R)$	is the net optical efficiency at wavelength $?_R$ of all receiving elements [unitless],
c	is the speed of light in air [m s^{-1}],
$?$	is the bin duration [s],
A	is the area of the receiving telescope [m^2],
$?(?_T,?_R)$	is the backscatter cross section [m^{-1}] of the volume element for the laser wavelength $?_T$ at Raman shifted wavelength $?_R$ [m^{-1}],
$?(?,z')$	is the extinction coefficient at wavelength $?$ at range z' [m^{-1}].

Using this relation, the number of photon counts expected from the received signal can be determined and the vertical profiles of the atmospheric properties can be obtained. It should be noted that return signals for the LAPS system using Equation 2.1, $P_T(?_T)$ are the time-averaged values for transmitted power at wavelength, $?_T$. It becomes apparent from the examination of the lidar equation that the Raman scattering techniques, which use the ratio of the signals at two wavelengths, greatly simplifies the measurement of the various parameters. In the above equation $?_R(?_R)$ is commonly known as the geometrical form factor and is critically dependent upon the details of the receiver optics. The analysis of the near field data (<800 m) is also important, because overfilling of the detector causes the effective profile of the received signal to be distorted [Mulik, et. al., 2000]. This signal distortion can be corrected by normalizing the detected signal to the actual received signal calculated using the geometry of the optics.

2.2.3 Water Vapor Measurement Technique

Water vapor concentration is a fundamental property of the atmosphere and provides us with information about some of the most important properties of our environment. It is a primary factor in the distribution of heat energy over the globe because of the latent heat taken up and given off during phase changes. Water vapor is also an excellent tracer of the local atmospheric dynamics. The largest concentration of atmospheric water vapor is found in the lower atmosphere and its concentration decreases with increasing altitude. The earliest Raman lidar measurements to yield the spatial distribution of water vapor in the atmosphere were performed by Melfi et al. (1969) and Cooney (1970). They used a frequency-doubled Q-switch ruby laser and normalized their

water vapor return using the nitrogen vibrational Raman return. The LAPS instrument measures the water vapor mixing ratio by taking the ratio of the signals from the 1st Stokes vibrational Raman shifts for water vapor and nitrogen. Profiles of water vapor can be obtained during the day (295/284) and the night (660/607) with the ultraviolet and visible laser wavelengths. LAPS has the capability of obtaining day time measurements by operating in the 'solar blind' spectral interval, between 230 and 300 nm, where stratospheric ozone absorbs the incoming radiation and limits the strong sky background radiance. The water vapor mixing ratio is expressed by taking the ratio of its number density to the number density of ambient air and multiplying by a calibration constant. The equation to obtain vertical profiles of water vapor at visible wavelengths is,

$$W(z) \propto K_{cal} \frac{S_{H2O}(z)}{S_{N2}(z)} \qquad [2.2]$$

where,

S_{H2O} is the received signal from the vibrational Raman shift of H_2O at 660 nm,
S_{N2} is the received signal from the vibrational Raman shift of N_2 at 607 nm,
K_{cal} is a calibration constant.

The calibration constant, K_{cal}, is obtained by fitting the ratio of the return signals of H_2O and N_2 with the data obtained from radiosondes balloons for water vapor at the same time. Since we are taking the ratio of the two signals and the numerator and the denominator have the same transmit wavelength most of the terms in the lidar equation cancel providing a simpler equation [Esposito, 1999].

$$\frac{P_{H20}(z)}{P_{N2}(z)} = \frac{\tau_R(\tau_{H2O})}{\tau_R(\tau_{N2})} \frac{\tau(\tau_T, \tau_{H2O}, z)}{\tau(\tau_T, \tau_{N2}, z)} \frac{\exp\left[-\int_0^z \alpha(\tau_{H2O}, z)\right] dz}{\exp\left[-\int_0^z \alpha(\tau_{N2}, z)\right] dz} \quad [2.3]$$

The extinction coefficient is assumed to equal the sum of the scattering due to molecules, scattering due to aerosols along the path, and the absorption by ozone. A constant, K_{system}, is introduced to simplify the calculation [Esposito, 1999].

$$\frac{P_{H_20}(z)}{P_{N2}(z)} = k_{system} \frac{\exp\left[-\int_0^z (\tau_m(\tau_{H2O,}\, z) + \tau_a(\tau_{H2O,}\, z) + \tau_{O3}(\tau_{H2O,}\, z))\right] dz}{\exp\left[-\int_0^z (\tau_m(\tau_{N2,}\, z) + \tau_a(\tau_{N2,}\, z) + \tau_{O3}(\tau_{N2,}\, z))\right] dz} \quad [2.4]$$

where,

$\tau_m(\tau_x,z)$ is the attenuation due to molecular scattering at wavelength τ_x,
$\tau_a(\tau_x,z)$ is the attenuation due to absorption and scattering of aerosols at wavelength τ_x,
$\tau_{O3}(\tau_x,z)$ is the attenuation due to ozone absorption at wavelength τ_x.

Since the differences between the absorption and scattering due to aerosols at the two wavelengths are small, they can be neglected, or treated as having a τ^{-1} dependence as an approximation,

$$\frac{P_{H20}(z)}{P_{N2}(z)} = k_{system} * \exp\left[-\int_0^z (\tau_m(\tau_{H2O,}\, z) + \tau_m(\tau_{N2,}\, z) + \tau_{O3}(\tau_{H2O,}\, z) + \tau_{O3}(\tau_{N2,}\, z))\right] dz \quad [2.5]$$

Equation 2.5 has to be corrected for molecular scattering and ozone absorption at the Raman shifted wavelengths in order to obtain an accurate water vapor measurement. The molecular scattering at each wavelength is given as [Esposito, 1999],

$$?_x K(z) ? ?\int_0^z ?_m(?_x, z?)dz?? ?_x ?\int_0^z ?NH?1 ? \exp?\frac{?? z??}{? H ??}?dz?? \quad [2.6]$$

$$H ? \frac{kT(z)}{mg} \quad [2.7]$$

$$T(z) ? To ? ? z \quad [2.8]$$

where,

N is the number density at ground level,
k is Boltzman's constant (1.380658 x 10^{-34}),
m is average mass per molecule,
g is gravitational acceleration,
To is the surface temperature,
? is the lapse rate of -6.5 K/km (valid only for the lower 10 km),
$?_x$ is the Rayleigh scattering cross-section at the x^{th} Raman shifted wavelength.

The molecular component of the signal loss can thus be removed from the data based upon the molecular scattering cross sections and the fractional abundance of N_2 and O_2,

$$W(z) ? K * \frac{S_{H2O}(Z)}{S_{N2}(Z)} \exp(?_{H2O} ? ?_{N2}) K(z) \ . \quad [2.9]$$

The water vapor mixing ratio calculated from the 1^{st} Stokes vibrational Raman shift of the visible transmitted beam (532 nm) does not need to be corrected for ozone absorption and hence the above equation, corrected for molecular scattering is used.

Since LAPS obtains profiles of water vapor in the daytime by using the *solar-blind* region, some of the transmitted radiation is absorbed by tropospheric ozone and hence correction for ozone absorption is necessary. By measuring the Raman backscatter return of O_2 at 277 nm and N_2 at 284 nm, it is possible to obtain the total ozone column density at low altitudes. Applying the Beer-Lambert law to this ratio of O_2 and N_2 leads to the following expression [Renault et al, 1980] for ozone column density,

$$\frac{S_{O2}}{S_{N2}} ? \frac{O_2}{N_2} \exp(?C(z)), \qquad [2.10]$$

where C(z) is the optical depth for ozone and is,

$$C(z) ? (? _{O_2} ? ? _{N_2}) ? \int_0^z O_3 dz \quad ? \ln ? \frac{S_{O2}}{S_{N2}} ? . \qquad [2.11]$$

The UV water vapor mixing ratio, which has been corrected for ozone absorption, can be expressed in the form,

$$w(z) ? K \frac{S_{H2O}(z)}{S_{N2}(z)} ? \frac{S_{O2}(z)}{S_{N2}(z)} ? ^{\frac{? _{H2O?} ? _{N2}}{? _{N2?} ? _{O2}}} . \qquad [2.12]$$

2.2.4 Ozone Measurement Technique

Ozone measurements are obtained by a DIAL (Differential Absorption Lidar) analysis of the Raman shifts of N_2 (284 nm) and O_2 (277nm), which occur on the steep side of the Hartley absorption band of ozone. Taking the ratio of the return signal from the Stokes Raman shifted signal from nitrogen molecules in the scattering volume, the lidar equation reduces to [Balsiger et al, 1996],

$$\frac{P_{O2}(z)}{P_{N2}(z)} = \frac{\sigma_R(\lambda_{O2})}{\sigma_R(\lambda_{N2})} \frac{\sigma(\lambda_T, \lambda_{O2}, z)}{\sigma(\lambda_L, \lambda_{N2}, z)} \frac{\exp\left[-\int_0^z [\sigma(\lambda_{O2}, z')]dz'\right]}{\exp\left[-\int_0^z [\sigma(\lambda_{N2}, z')]dz'\right]} \qquad [2.13]$$

Choosing a system constant, ksystem,

$$k_{system} = \frac{\sigma_R(\lambda_{O2})}{\sigma_R(\lambda_{N2})} \frac{\sigma(\lambda_T, \lambda_{O2}, z)}{\sigma(\lambda_T, \lambda_{N2}, z)} = \frac{\sigma_R(\lambda_{O2})}{\sigma_R(\lambda_{N2})} \frac{\sigma_{O2}}{\sigma_{N2}} \frac{[O2]}{[N2]} \qquad [2.14]$$

where,

σ_x is the Raman cross-section of x at the laser wavelength,
[X] is the number density concentration of x in the atmosphere.

and also neglecting the attenuation due to scattering and absorption of aerosols further simplifies the above equation to [Esposito, 1999],

$$\frac{P_{O2}(z)}{P_{N2}(z)} = k_{system} * \exp\left[-\int_0^z [\alpha_m(\lambda_{O2}, z') - \alpha_m(\lambda_{N2}, z')]dz\right] \exp\left[-\int_0^z [\alpha_{O3}(\lambda_{O2}, z') - \alpha_{O3}(\lambda_{N2}, z')]dz\right] \qquad [2.8]$$

where,

$\alpha_m(\lambda_x, z)$ is the attenuation due to molecular scattering at wavelength λ_x,
$\alpha_{O3}(\lambda_x, z)$ is the attenuation due to ozone absorption at wavelength λ_x.

The number density of ozone in a scattering volume is calculated by differentiating the integrated ozone number density corrected for molecular scattering [Esposito, 1999] and is,

$$[O_3(z)] = \frac{d}{dz}\left[\ln\left(\frac{P_{O2}(z)}{P_{N2}(z)}\frac{1}{k_{system}}\right)\right] * \frac{1}{\left(\frac{1}{P_{N2}} - \frac{1}{P_{O2}}\right)} - \frac{\left(\frac{1}{P_{O2}} - \frac{1}{P_{N2}}\right)}{\left(\frac{1}{P_{N2}} - \frac{1}{P_{O2}}\right)}K(z) \qquad [2.9]$$

From the above equation it is possible to obtain the ozone concentration only after the first bin, i.e., approximately 113 m above ground level and that value has a large associated error. To incorporate ground level measurements into the lidar profiles, surface measurements are used. The reader is referred to Mulik [2000] for a detailed explanation of this procedure.

2.3 Wind Profiling Radar

The LAP-3000 wind profiling radar is an atmospheric remote sensing instrument and provides profiles of wind speed and direction up to a height of 4 km. The U.S. National Oceanic and Atmospheric Administration (NOAA) developed the technology that is the basis for the instrument, and in 1991, Radian International (now Vaisala) and Sonoma Technology, Inc. were licensed to develop and commercially produce the LAP-3000 (Lower Atmosphere Profiler Model 3000).

The generic name “profiler” comes from the radar’s ability to provide data at many heights of the atmosphere at the same time, thus giving a profile of the atmosphere. Fundamentally, the wind profiler is a pulse Doppler radar. It transmits a pulse of electromagnetic energy in a particular direction and receives the electromagnetic energy that is scattered back when the pulse encounters a “target”. A small portion of the

backscatter energy will return to the radar receiver, and is then used to measure the various parameters. The instrument provides a sequential set of profiles of the atmosphere backscatter signals, which are sampled at equally spaced time intervals after each transmitted pulse to create the profile at equally spaced heights. These intervals, during which the backscatter is sampled, are called range gates. The energy is scattered back from a volume rather than a single point and the radial length of this volume is determined by the range gate. The pulse length is usually short compared with the travel time twice through the range bin. The radar height assigned to the range gate is at the center of the resolution volume. The wind profiling radar uses refractive irregularities and particulates in the atmosphere as targets. The maximum backscatter occurs when the scattering irregularities are about half the size of the radar wavelength. A refractive irregularity can be considered as anything that comes in the path of the transmitted wave and changes the course of the wave through the medium. The atmosphere is turbulent and this motion creates variations in temperature, humidity and pressure called eddies. These eddies result in refractive irregularities that the profiler uses as targets. Since the eddies are carried by the wind field, their Doppler velocities provide measurements of the wind velocity. The profiler computes height by using the time interval between transmission of the pulse and reception of the echo. The wind speed and direction are determined by measuring the Doppler shift in the frequency of the return signal. The wind profiling radar measures the radial Doppler velocity in the North-South and East-West planes, as well as, in the vertical direction in order to compute the wind velocity. A frequency higher than the transmitted frequency indicates motion of the wind towards the profiler and a frequency lower than the transmitted one indicates that the wind is moving away

from the profiler. These shifts in the frequency of the backscattered signal are translated into wind velocity components. The profiler makes measurements in as many as five directions in order to compute the wind speed and direction. As seen in Figure 2.5 four oblique beams are tilted about 23.5^0 from the vertical beam and directed in four orthogonal directions. The transmitted beam is directed to a phased-array antenna that has a beam width of about nine degrees. The beam sequence, including the number of beams is user controlled and should contain the vertical beam and at least two tilted orthogonal beams. A sample is obtained by a complete rotation through a beam sequence and the samples are processed together to obtain an average for each range gate.

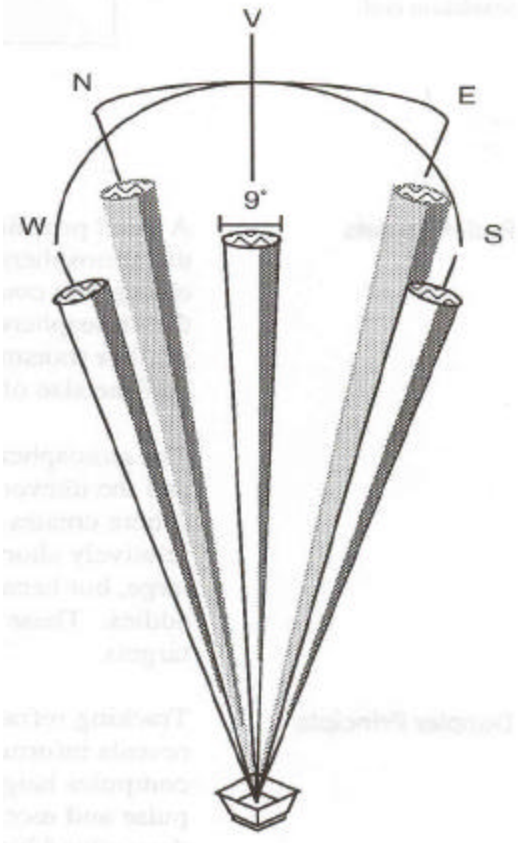

Figure 2.5 Antenna beam sequence of the profiler [Radian, 1997].

The wind profiler is operated at 915 MHz and has a wavelength of 32.8 cm. This wavelength detects the small refractive features that are most abundant in the lower atmosphere as targets and allows for a relatively small antenna size. The aperture of the antenna determines the beam width and antenna gain. The antenna gain is directly proportional to the aperture and hence the small aperture of the antenna produces a gain of about 25 dBi. The height of coverage increases with higher transmitted power, and this profiler's amplifier has a peak-power output of 600 Watts. The typical performance specifications of the profiler are given in Table 2.5.

Table 2.5 Performance characteristics of the profiler.

Minimum measurement height	120 m
Maximum measurement height	2 to 5 km
Vertical resolution: With 400ns pulse With 700ns pulse With 1400ns pulse With 2800ns pulse	 60 m 100 m 200 m 400 m
Wind speed accuracy	<1 m/s
Wind direction accuracy	<10 degrees

The pulse width is operator controlled and plays an important role in maximum and minimum height coverage. A longer pulse increases both the maximum and minimum height coverage of the profiler, while a shorter pulse duration provides better range resolution and lowers the minimum height measured. The inter-pulse period is another user-controlled parameter and is the time interval between any two pulses. Decreasing the inter-pulse period increases the profiler's height coverage. It is necessary to choose appropriate values of pulse duration and inter-pulse period to obtain the desired

range and resolution. A typical set of operating parameters for the profiler is given in Table 2.6. The sampling delay is the time interval between the end of the transmit pulse and the first range gate, and determines the first height sampled by the profiler.

Table 2.6 Operating parameters of the profiler.

Pulse width	0.7 ?s
Pulse repetition period	25 ?s
Number of spectral points	64
Maximum radial velocity	?10 m/s
Height range (sampled)	120 m to 3 km
Sample spacing	100 m
Averaging time	Variable

The samples that are received from the range gates undergo two stages of signal processing. In the first stage, the samples are averaged in the time-domain. A longer averaging time improves the data quality but it is possible to use an averaging time that is so long that it reduces the highest speed or radial wind measurements. After averaging, an offset of the DC voltage is removed by mathematical signal processing techniques and then the Fast Fourier Transform (FFT) is used to convert the samples from the time domain to the frequency domain. The FFT results are then incoherently averaged. The next segment of signal processing uses a technique called “windowing” which is used to reduce some of the mathematical artifacts of the FFT processing. After windowing, mathematical signal processing techniques are used to remove ground clutter, which is due to backscatter from stationary targets. The profiler gives information for successive layers in the atmospheric boundary layer, creating a profile of wind data. It is a flexible and useful instrument, and can operate at remote sites unattended for long periods of

time. Figure 2.6 is a descriptive diagram of the various components and their location within the system.

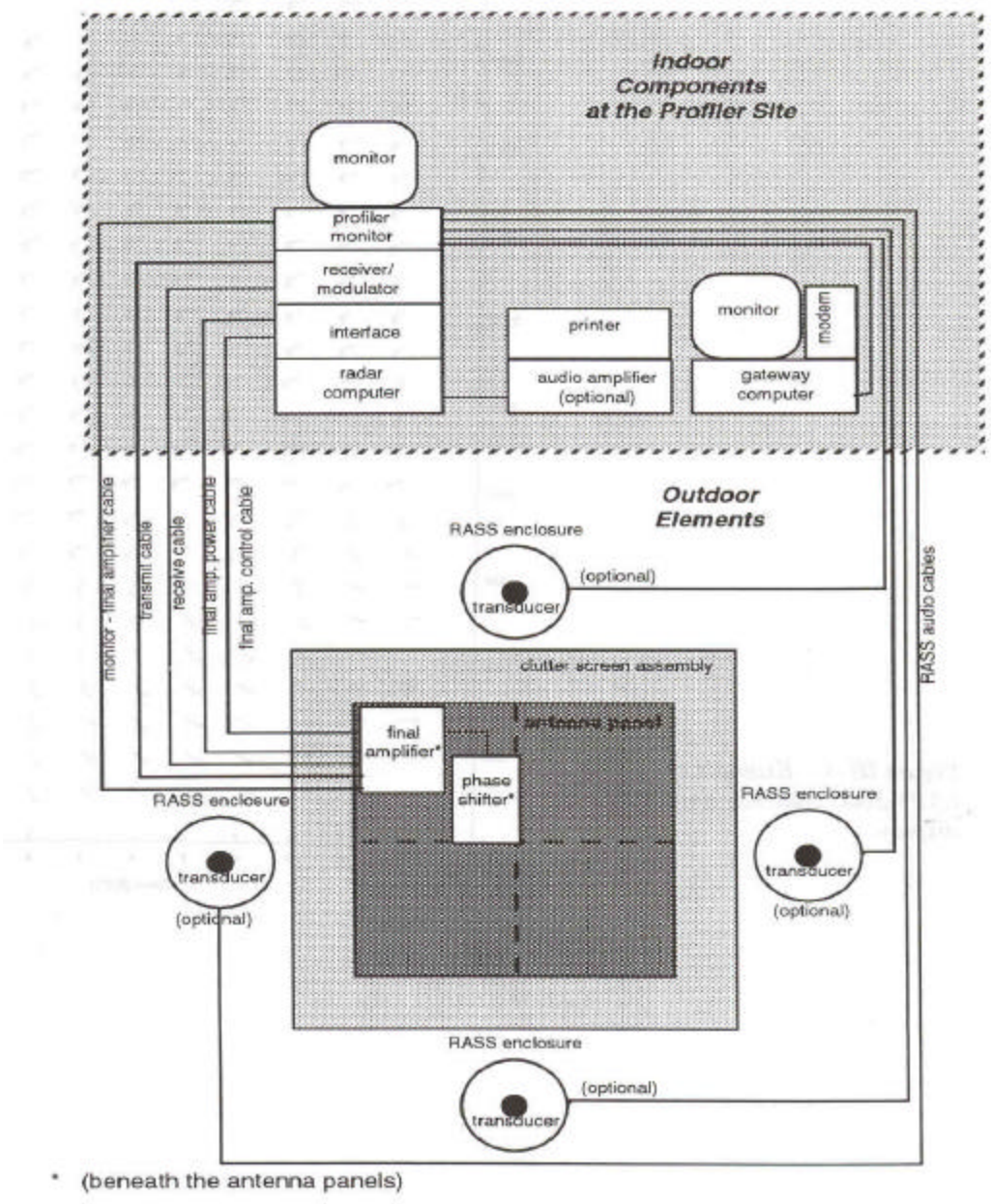

Figure 2.6 Block diagram of LAP-3000 profiler/RASS hardware components [Radian, 1997].

2.4 Radio Acoustic Sounding System (RASS)

The Radio Acoustic Sounding System (RASS) provides profiles of virtual temperature using vertically directed acoustic waves. The wind profiling radar/RASS is shown in Figure 2.7. The RASS system consists of four acoustic sources, one on each side of the profiler, which transmit vertically directed acoustic waves that are used as targets by the profiler. The backscatter signal from the Doppler radar detects the transmitted acoustic frequency in the signal of scattering refractive effects produced by

Figure 2.7 Wind profiling radar/RASS at the Philadelphia Baxter site (photo credit, C.R. Philbrick).

the acoustic wave. The speed of propagation of the acoustic wave is then determined from the Doppler shifted frequency. Virtual temperature profiles are directly calculated from the speed of sound. The propagation speed of the acoustic wave (C_a) depends on the temperature and moisture composition of the atmosphere. The speed of the acoustic wave is related to the virtual temperature (T_v) by,

$$T_v = (C_a/20.047)^2 \quad [2.10]$$

The virtual temperature is related to air temperature (T) by,

$$T_v = T(1+0.61r) \quad [2.11]$$

where,

r is the mixing ratio of unsaturated air

The typical performance specifications of RASS are given in Table 2.7.

Table 2.7 Performance characteristics of RASS.

Minimum measurement height	120 m
Maximum measurement height	1 to 2 km
Vertical resolution: With 400ns pulse With 700ns pulse With 1400ns pulse With 2800ns pulse	 60 m 100 m 200 m 400 m
Minimum vertical resolution	60 m
Temperature accuracy	1^0 C

The RASS has the same range resolution and minimum height coverage as the profiler. The RASS's maximum height coverage is limited to only 2 km as the atmosphere strongly scatters acoustic waves and strong winds can transport the acoustic signal out of vertical alignment with the radar antenna beam. All the operating parameters for the RASS are similar to the profiler and are given in Table 2.8.

Table 2.8 Operating parameters of RASS.

Pulse repetition period	20 ?s
Number of spectral points	2048
Height range (sampled)	120 m to 1.5 km
Sample spacing	60 m
Averaging time	10 minutes

The RASS enclosure as shown in Figure 2.6 consists of a transducer that transmits the acoustic signal. The transducer is a horn-loaded compression driver positioned at the focus of a 1.23 m parabolic reflector. Virtual temperature measurements are not possible during precipitation, high winds and strong turbulence. Turbulence disrupts the coherence of the acoustic wavefront used for virtual temperature measurements, reducing the range obtained. High winds affect the virtual temperature measurement by increasing the pressure waves from ground clutter and reducing the range of measurement by displacing the acoustic signal away from the beam.

CHAPTER 3

LOW-LEVEL JETS

3.1 Atmospheric Boundary Layer

The boundary layer is defined as that part of the troposphere that is directly influenced by the presence of the Earth's surface, and responds to surface forcings such as surface heating, dynamics of global and local weather systems, frictional drag, heat transfer and terrain induced flow modification [Stull, 1997]. The thickness of the boundary layer varies diurnally, and typically ranges from a few hundred meters during the night to as much as a few kilometers during the day. The remainder of the troposphere is usually called the free atmosphere where the geostrophic wind is a reasonable approximation of the actual wind. Typically, in the northern hemisphere, the wind blows at right angles to the pressure gradient, with high pressure to its right and low pressure to its left, and its speed is proportional to the magnitude of the pressure gradient. Only by doing this can the forces balance and the air keep its acceleration to a minimum. This balance of forces is called geostrophic balance. The wind speed and direction, which is induced as a consequence of the geostrophic balance, is called the geostrophic wind.

Over land surfaces the boundary layer has a well-defined structure and can be divided into the mixed layer, the residual layer, and the stable boundary layer. The bottom-most region of the boundary layer is called the surface layer. In this lowest region, the fluxes and stress vary by less than 10% of their magnitude, and it remains relatively unchanged during day and night [Stull, 1997].

The mixed layer usually begins to develop just after sunrise and dies out around sunset when the solar heating stops. A shallow well-mixed layer begins to develop soon after sunrise when the breakdown of the nocturnal inversion occurs because of surface heating. As the solar heating increases and the ground becomes warmer, the depth of the mixed layer begins to grow and it is characterized by intense mixing as thermals of warm air rise from the ground. The depth of the mixed layer increases and reaches its maximum at mid to late afternoon when surface temperatures are greatest. Surface heating usually convectively drives the turbulence in the mixed layer, although a nearly well mixed layer can form in regions of strong winds [Stull, 1997]. Thermals of warm air rising from the ground are due to the transfer of heat from the warm ground surface, while radiative cooling from the top of the cloud layer causes thermals of cool air to sink from cloud tops. Wind speeds are subgeostrophic throughout the mixed layer. The middle portion of the boundary layer has nearly constant wind speed and direction. The wind speeds are seen to decrease towards zero near the ground under usual conditions. Since most of the pollutants sources are near the Earth's surface, the pollutant concentrations build up and remain high in the mixed layer, while their concentrations remain relatively low in the upper regions of the atmosphere. The structure of the boundary layer as it evolves diurnally is shown in Figure 3.1.

The turbulence in the well-mixed layer begins to decay as the thermals cease to form at around sunset. The resulting layer of air is sometimes called the residual layer because its initial mean state variables and concentration variables are the same as those of the recently decayed convective mixed layer [Stull, 1997]. Since the wind speed remains fairly low in the mixed layer during the daytime, the pollutants and passive

tracers dispersed in the daytime mixed layer will remain aloft in the residual layer during the night. It is important to note that the pollutants that are aloft may react with other pollutants during the night to create certain compounds that were not originally emitted and may be more stable for long distant transport in the cooler upper layers. Also, as the convective mixed layer begins to form the following day, these pollutants precursor concentrations can be mixed down to the ground, and in the presence of solar radiation can trigger photochemical reactions increasing the pollutant concentrations at the surface. Studying the transport mechanisms in the residual layer is important because the pollutant concentrations there can be transported hundreds of miles into other regions, contributing to the pollutant concentrations observed the following day at those locations.

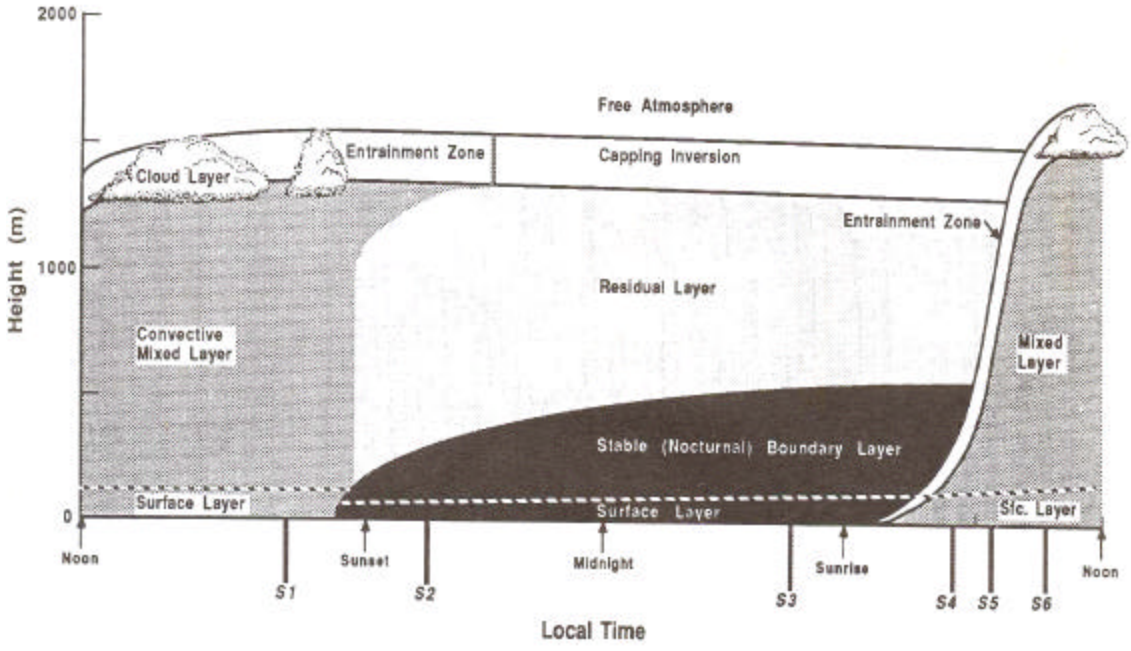

Figure 3.1 Schematic showing the diurnal variation of the boundary layer structure [Stull, 1997].

As the night progresses, the bottom of the troposphere is transformed by its contact with the ground into the stable boundary layer or the nocturnal boundary layer. Usually during the night, this region is highly stable as the temperature increases with height, and is classified as temperature inversion or nocturnal inversion. The nocturnal boundary layer becomes stably stratified due to the positive temperature gradient formed when the surface is cooler than the air. As seen in Figure 3.1 the stable boundary layer blends into the residual layer. The nocturnal boundary layer is characterized by stable air with weaker, sporadic turbulence. Typically, stability decreases smoothly towards neutral with height, with the greatest static stability near the ground. This stable layer effectively decouples the surface friction from the wind field of the lower troposphere. It is seen in many cases that the wind speeds in the stable boundary layer increase with height and reaches a maximum near the top of the stable boundary layer.

3.2 Low-Level Jets

One of the most significant and interesting processes in the evening boundary layer transition over flat terrain is the development of the low-level jet (LLJ), or nocturnal jet. These low-level wind maximums in the boundary layer occur under a number of rather different circumstances. Typically, as the nocturnal inversion deepens, the wind speed is seen to increase with height, reaching a maximum above the top of the stable layer. This region of wind is observed to have speeds greater than the geostrophic speed, and is called the low-level jet. Figure 3.2 shows the characteristics of the wind field associated with a low-level jet over Philadelphia on July 25th 2001. They generally form during the nighttime over land under clear sky conditions but are destroyed just

after sunrise, at which time solar heating and vertical mixing erode the developed wind field [Clark, 2001]. Low-level jets are not rare phenomena, and they have been observed on every continent. LLJ's typically occur in regions to the east of a large mountain range or where large land-sea temperature gradients exist. At middle latitudes, LLJ's are more frequent in the summer months [Stensrud, 1996]. A large number of studies have been done to study these jets and investigators have associated these jets with a number of atmospheric processes [Pitchford et al, 1962; Seaman et al, 1998; Reitebuch et al, 2000; Banta et al, 2001; Clark et al, 2001]. In the Unites States, the LLJ's occurring over the

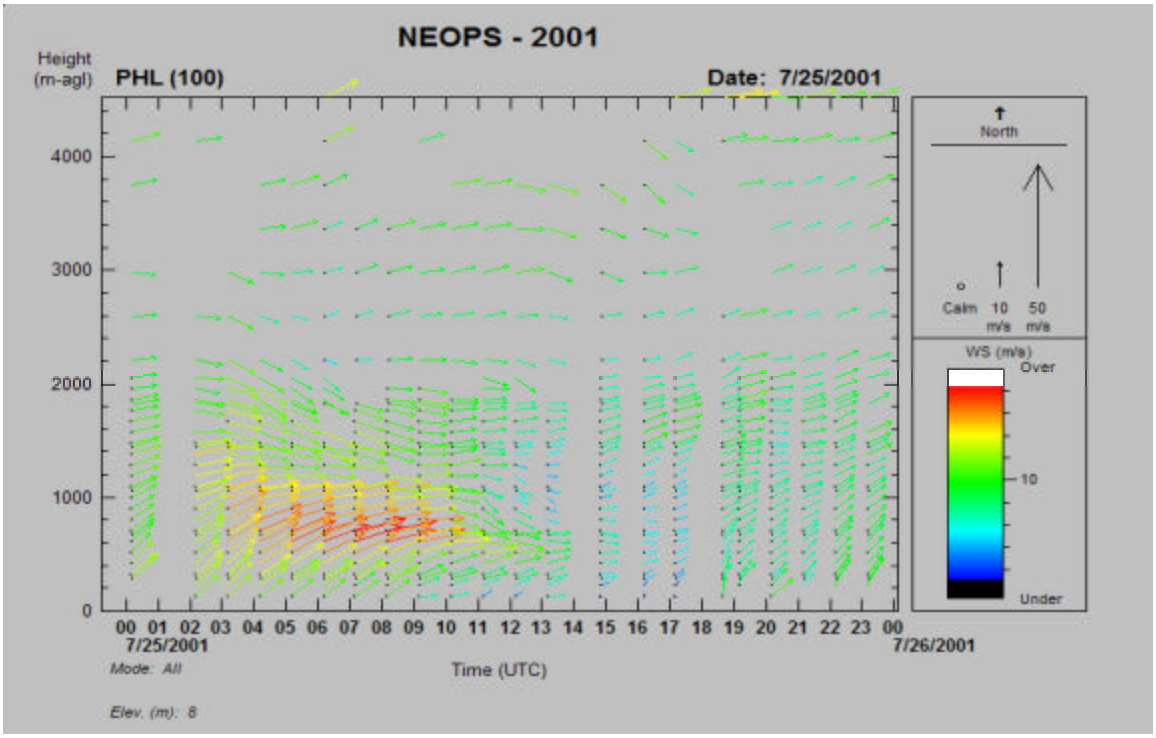

Figure 3.2 Low-level jet observed over Philadelphia on July 25 2001.

Great Plains region have been studied more than any other location. Studies over that region have revealed a strong influence of LLJ's on precipitation and other severe weather conditions. Studies of low-level jets are important, because, in addition to their

influence on atmospheric processes, they have the ability to transport moisture and pollutants over long distances.

3.2.1 Mechanisms of Low-Level Jet Formation

There are a number of physical mechanisms that have been developed to explain evolution of LLJ's. Some of these include [Stull, 1997],

- Inertial oscillations
- Baroclinicity associated with sloping terrain
- Fronts
- Advective accelerations
- Mountain and valley winds
- Synoptic-scale baroclinicity associated with weather patterns.

In the boundary layer, the first two mechanisms are considered to be the most widely seen as a source for generating LLJ's. These mechanisms give us a better understanding of the evolution of the LLJ in terms of time, strength of the wind, and height of the wind maximum.

3.2.1.a Inertial Oscillation

This mechanism was explained by Blackadar in 1957, and accounts for both the daily oscillations in jet intensity and for the significantly supergeostrophic (greater than geostrophic) velocities observed during the nighttime. He related the evolution of the jet to the growth of the nocturnal inversion. During the daytime, the strong frictional drag at the ground and the strong vertical mixing maintains the wind at subgeostrophic speeds

through the convective boundary layer. At sunset, as the mixing ceases, the frictional effects are reduced significantly and the wind flow above the nocturnal inversion is decoupled from the surface friction. This decoupling disrupts the daytime balance of horizontal forces and produces an acceleration of flow just above the nocturnal inversion. An inertial oscillation is induced from the imbalance between the pressure gradient and Coriolis forces, and causes the frictionless stream of air to reach supergeostrophic speeds after several hours. Typically at midlatitudes the inertial oscillation is about 17 h, and the LLJ formed would produce a wind speed maximum on the order of 6 h after the cessation of turbulent mixing [Hoxit, 1975].

3.2.1.b Baroclinicity Over Sloping Terrain

Theories other than the Blackadar's theory of inertial oscillations have been proposed which account in whole or part of the evolution of LLJ's. Let us consider Holton's analysis in 1967 for a mechanism that describes the nature of the LLJ as a response to the diurnal heating and cooling of the sloping terrain, which results in periodic variation in thermal wind and a consequent surface geostrophic wind oscillation. The thermal wind relationship is given by [Holton, 1972],

$$\frac{?U_g}{?z} ? \frac{? g}{f_c T} \frac{?T}{?y} \qquad [3.1]$$

$$\frac{?V_g}{?z} ? \frac{g}{f_c T} \frac{?T}{?x} \qquad [3.2]$$

where,

U_g, V_g	are the eastward and northward component of geostrophic wind respectively,
T	is the absolute temperature,
g	is the acceleration due to gravity,
f_c	is the Coriolis parameter,
x, y	are the Cartesian coordinates towards the east and up respectively.

Consider the scenario of a late afternoon situation where solar insolation warms the ground and forms the well-developed mixed layer with near adiabatic lapse rate so that the west to east temperature gradient is negative near the ground and aloft. These negative geostrophic wind gradients along with the strong daytime mixing prevent the formation of the jet during the day. This is schematically shown in Figure 3.3a and 3.3b. During the nighttime, as seen in Figure 3.3c and 3.3d, the west to east temperature gradient reverses as the ground cools more quickly, and this reverses the thermal wind at

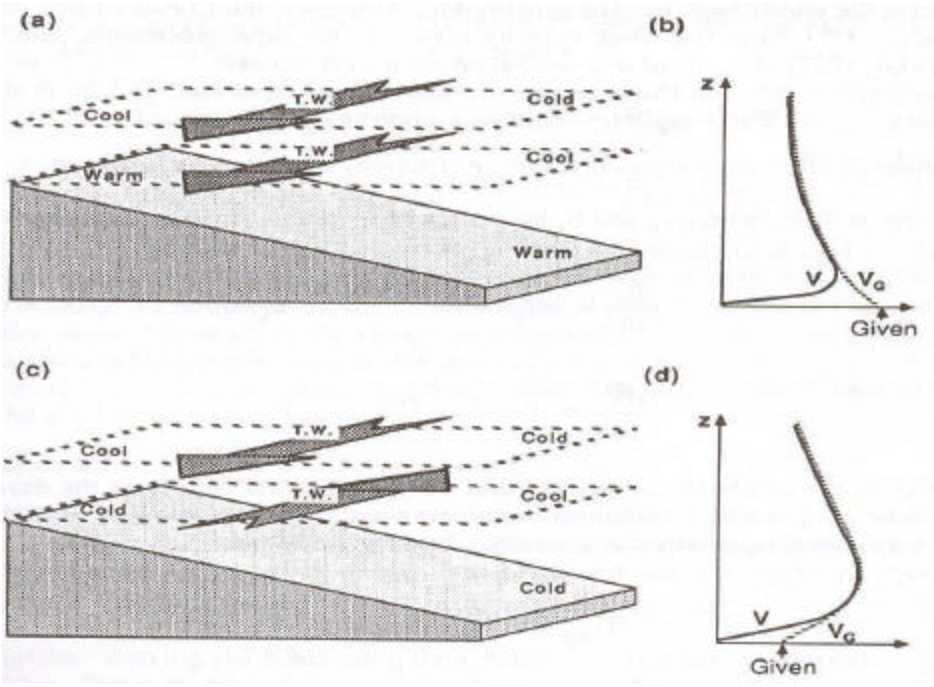

Figure 3.3 low-level jet formations due to thermal wind forcings over sloping terrain [Stull, 1997].

low altitudes in the stable boundary layer. Above the level of the inversion the gradient may again reverse such that the thermal wind remains unchanged. Also, since frictional forces tend to suppress the wind speeds near the surface, a jet is seen to form at the level near the nocturnal inversion. This theory does not explain the super-geostrophic wind formation but explains the growth of the jet at the top of the nocturnal inversion.

3.2.2 Characteristics of the Northeastern Low-Level Jet

A recurring feature of the NorthEast Particle and Oxidant Study (NE-OPS), conducted at the NEOPS site in Philadelphia, during the summers of 1999, 2001 and 2002, was the presence of nocturnal low-level jets. While not as strong or persistent as the Great Plains LLJ's, the formation mechanism was observed to be similar to the conceptual model of inertial oscillation explained by Blackadar. Clark et al (2001) explained that in the summertime, when the mid-Atlantic is under conditions of weak synoptic forcing, substantial gradients are produced in the boundary layer during the daytime due to differential surface heating between the coastal plain and the Appalachian leeside. These gradients support a near-surface geostrophic wind, but the frictional stress prevents the wind from achieving geostrophic balance. An ageostrophic wind is thus induced proportional to the frictional stress. With the development of the nocturnal inversion and the cessation of convective turbulence after sunset, the velocity field accelerates in an attempt to adjust to the mass field. This acceleration is subject to the Coriolis force and results in a shallow layer of faster moving air residing on top of the nocturnal inversion. At sunrise, solar heating and vertical mixing erode the wind field and the LLJ disappears. LLJ's forming over the mid-Atlantic are generally confined to a layer

between 200 m and 800 m, with the maximums in wind speed residing on top of the nocturnal inversion within the remnants of the previous day's convective mixed layer. Figure 3.4 shows the characteristic shape of the wind profile at heights between 200-800 m on 1 July 2002 observed at the Philadelphia Baxter site by the Penn State wind profiler. Just around sunset, 0000 UTC and 0100 UTC, the wind speeds are seen to remain at about 8 ms^{-1}. As the stable boundary layer begins to grow, the temperature inversion frees the upper region from the surface frictional drag and the wind speeds begin to increase with the maximum usually occurring at around 400 m. In this case, the fully formed jet with speeds reaching 14 ms^{-1} is observed at about 0800 UTC.

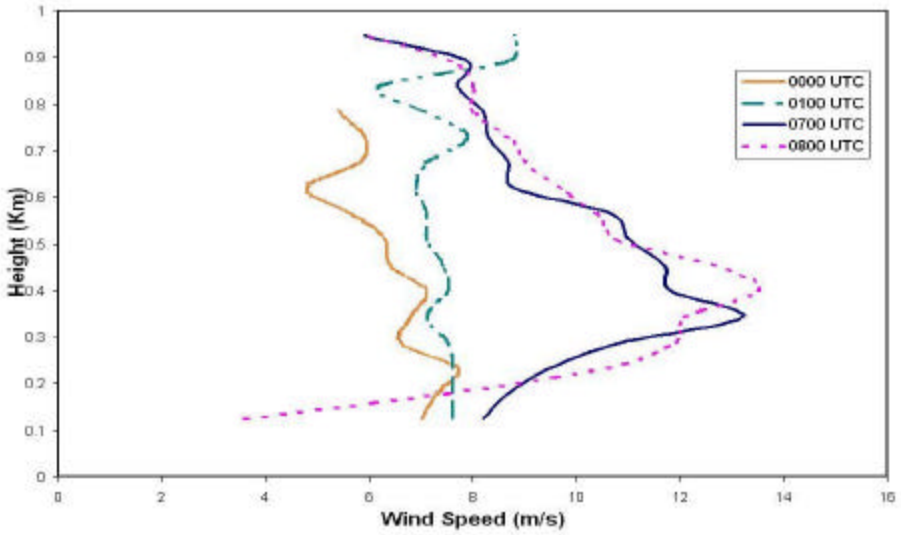

Figure 3.4 Evolution of the wind field above Philadelphia, on the night of July 1 2002.

Numerical models such as Meso-Eta and MM5 are capable of resolving certain general features of LLJ's, but it becomes necessary to integrate them with continuous remote sensing observations to obtain a more complete understanding of the evolution and the dynamics of the LLJ. The data obtained from the profilers at Rutgers University, NJ, and Ft. Meade, MD, (www.pofiler.noaa.gov/jsp/profiler.jsp) are used in conjunction

with the measurements from the NEOPS campaigns to characterize certain features of the jets observed along the northeastern region. We observed the signatures of LLJ's occurring on several nights as part of the NE-OPS investigations. These features are explained in the remainder of this section.

3.2.2.a Vertical Structure of the Jet

To obtain the characteristics of the jet it becomes necessary to clearly define a jet and develop criteria for describing jet observations. A jet observation for our case is defined, following Blackadar, as any significant, low level, maximum in vertical profiles of the wind speed. Bonner (1968) suggested a stringent set of criteria for the southerly Great Plains jet. He defined the criterion based on the minimum speed and the decrease in speed above the jet such that,

Criterion 1: The wind at the level of maximum wind must equal or exceed 12 ms^{-1} and must decrease by at least 6 ms^{-1} to the next higher minimum or the 3 km level, which ever is lower.

Criterion 2: The wind at the level of maximum wind must equal or exceed 16 ms^{-1} and must decrease by at least 8 ms^{-1} to the next higher minimum or the 3 km level, which ever is lower.

Criterion 3: The wind at the level of maximum wind must equal or exceed 20 ms^{-1} and must decrease by at least 10 ms^{-1} to the next higher minimum or the 3 km level, which ever is lower.

These criteria differed from Blackadar's, which only required that the speed of the level of maximum wind be at least 5 knots (2.6 ms^{-1}) greater than regions above and below.

Since the LLJ's observed over the northeast are not as strong as the Great Plains LLJ, a modified set of rules must be applied to quantify them. Based on the conventional criteria of Blackadar and Bonner, we have chosen to define the northeast LLJ as one in which the maximum wind speed at the jet core should be at least 3 ms^{-1} greater than the region above and below the core. We also define the LLJ to be the first wind maximum occurring above the surface and below the altitude of 1200 m. To obtain the vertical structure of the northeast low-level jet, the data from 1999, 2000, 2001, and 2002 were subject to the criteria stated above. The statistics of the distribution of the LLJ's height of maximum wind speed at the various heights of the boundary layer are shown in Figure 3.5. The data indicates that the majority of the jets have their maximum speed occurring in the region between 400 and 700 m. The number of jet speed maximums observed reduces with height except in the region between 900 m and 1000 m. Further studies will help us resolve the kind of conditions that make the jet speed maximums to occur at high regions. The data shown in the region higher than 1200 m is the cumulative number of jet speed maximums observed in the region between 1200 m and 2500 m. The data observed in this region are not boundary layer low-level jets. Mean maximum speeds and altitudes of the jet were determined for the NEOPS site in northeast Philadelphia with the data obtained over the fours years. Average maximum speeds varied over the years and so did the vertical structure of the jet. The jets had an average speed of about 16.3 ms^{-1}. Most of the low-level jets were seen to form in the region between 400 m and 1000 m.

Another characteristic feature of the jet was that its wind direction rotated from southwesterly to westerly with time. This characteristic rotation of the wind field with time is important for air chemistry because of its ability to change the trajectories of air

parcels reaching the region from upstream locations. Figure 3.6 shows a typical low-level jet seen over the northeast region having a jet maximum speed of 16 ms^{-1}, and lying within the characteristic region of 400 m to 1000 m.

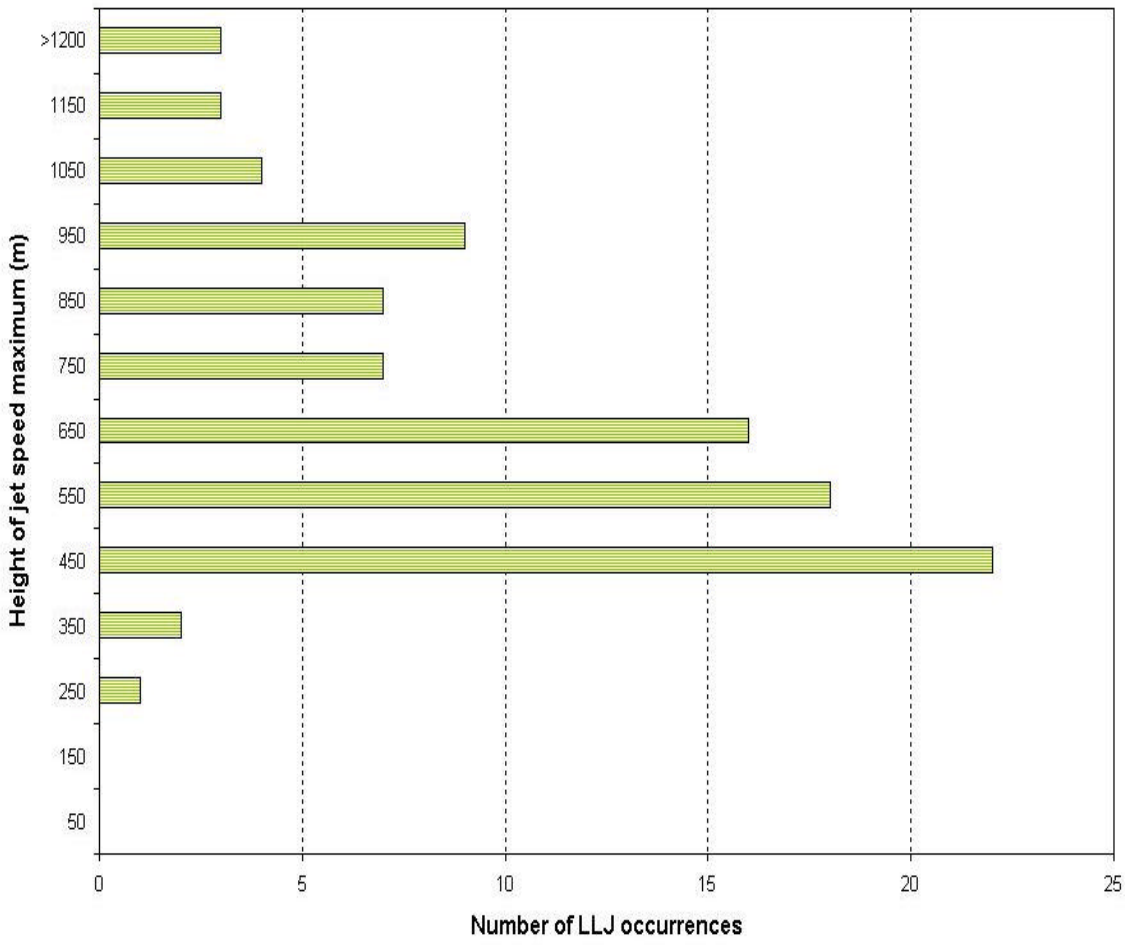

Figure 3.5 Distribution of the heights of jet speed maximum at the Philadelphia Baxter site.

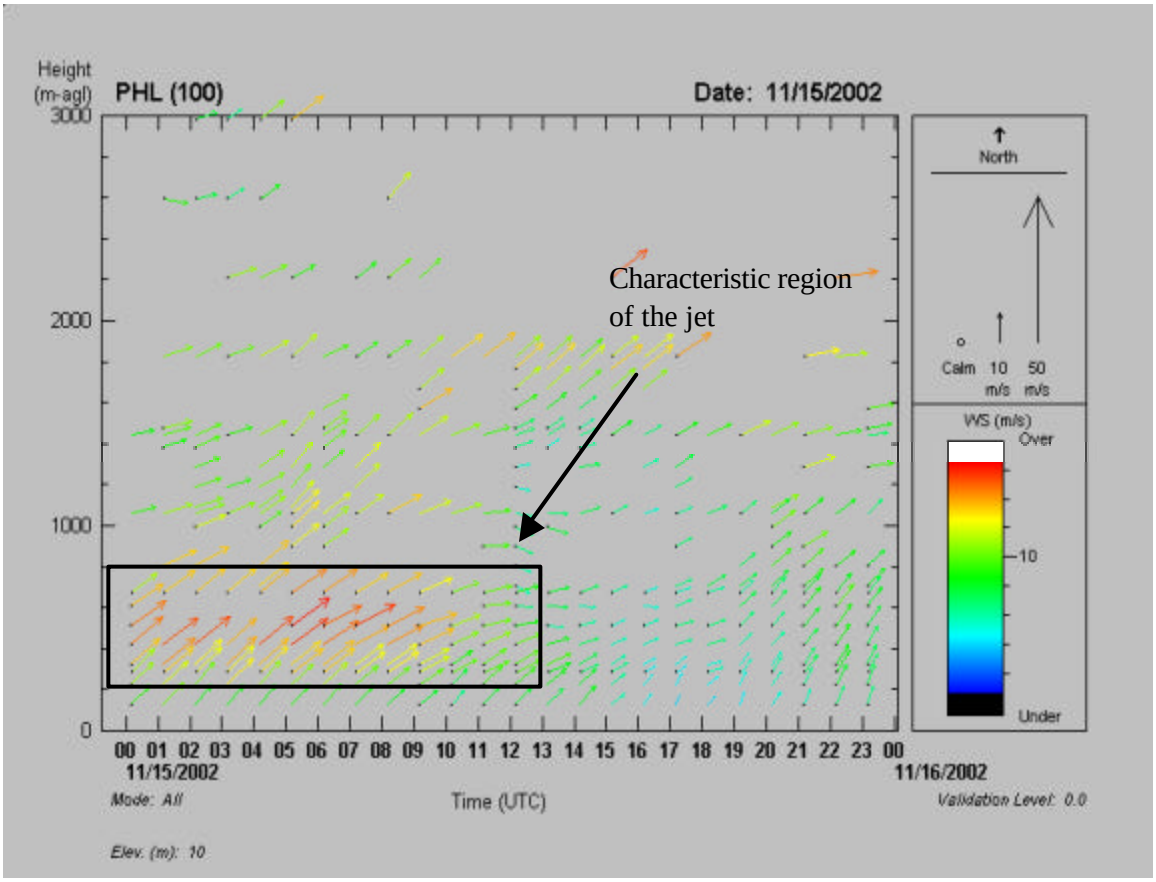

Figure 3.6 Characteristic LLJ observed over the northeast region.

3.2.2.b Relationship between Temperature Inversion and Wind Speed Maximum

Being considered the starting point for the development of the low-level jet, the nocturnal inversion is an entity that is understood to be important in describing wind flow patterns and wind profiles. The nocturnal inversion begins to form soon after sunset as a result of the loss of diurnal heating and convective mixing. Diurnal wind variations occur as the atmospheric mixing begins to decrease in the early evening. During the day winds are kept at a minimum because the strong vertical mixing couples the lower atmosphere viscosity to the surface. However, during sunset the mixing ceases, thus decoupling the atmospheric flow and allowing the speed of the boundary layer wind to respond to

existing pressure gradients. These increasing wind speeds generate a wind shear in the boundary layer. Blackadar (1957) showed that the development of turbulence at the top of the inversion occurs soon after this wind shear starts to form, initiating heat and momentum transfer processes, which transport both variables back to the surface. As the inversion begins to grow, a slight increase in the winds at the level of wind maximum occurs. The LLJ thus begins to form and resides on top of the nocturnal inversion. Figures 3.7a and 3.7b show the growth of the wind speed and the nocturnal inversion on July 1st 2002. The height of the wind speed maximum is seen to coincide with the height of the nocturnal inversion top. At about 1200 UTC (8 AM local) the inversion begins to break down as the surface begins to warm and the daytime temperature gradient is reestablished. The wind speed then returns to its normal daytime profile. To investigate the relationship further, data obtained at the Baxter site during 2002, was used to compare the height of the inversion with the height of the jet speed maximum. From this analysis, the inversion can be said to define the height of the jet wind speed maximum. Also, the inversion maximum was only taken between 8 P.M and 8 A.M local time. Comparison of the inversion height with the LLJ wind maximum was done for the 30 cases in 2002. The level of maximum wind was above the inversion height in 41% of the cases, below in 15%, and at about the same height as the inversion top on 44% of the cases.

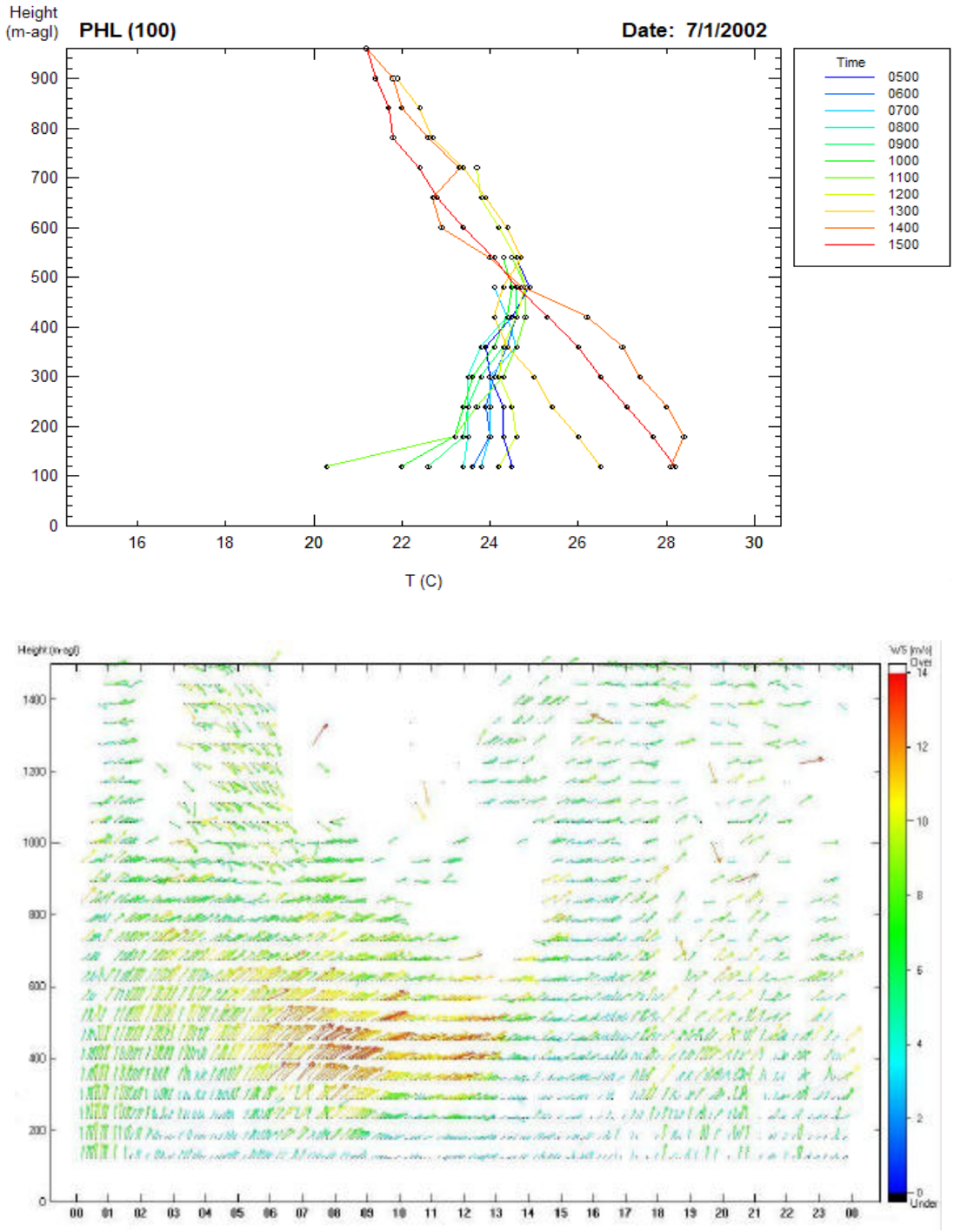

Figure 3.7 (a) Virtual temperature profile on July 1 2002 at the Baxter site **(b)** Wind Profile on July 1 2002 at the Baxter Site

3.2.2.c Horizontal Extent of the Jet

To delineate the horizontal structure of the jet, observations of wind speed and direction were obtained from profilers located at the NEOPS site in northeast Philadelphia, Fort Meade, MD, and New Brunswick, NJ. A total of 21 cases were chosen in the summer of 2002 to compare the presence of LLJ's at the three sites. The cases showed the presence of jets with maximum speeds occurring at the same hour on most nights at all the three sites. This indicates that the jet has a structure that extends across these three sites. Also, the time and height of the maximum in wind speed were approximately the same at all the three sites. At speeds of 15 ms^{-1}, the LLJ possesses the capability to transport parcels more than 200 km during the night. Additional data obtained from sounders around the region will help us to determine the exact north-south and east-west structure of the jet. Figure 3.8 shows the location of the three sites and the intercity extent of the jet. The dates compared and the presence of the jets at the three sites is shown in Table 3.1.

? Fort Meade
? Northeast Philadelphia
? New Brunswick

Figure 3.8 Location of the three sites whose data indicates an intercity extent of the northeast jet.

Table 3.1 Low-level jet observations at the 3 sites during summer 2002.

DATE	NORTHEAST PHILADELPHIA	NEW BRUNSWICK - RUTGETS	FORT MEADE
22 JUNE	**X**	**X**	-
23 JUNE	**X**	**X**	**X**
24 JUNE	**X**	**X**	-
27 JUNE	**X**	**X**	**X**
1 JULY	**X**	**X**	**X**
2 JULY	**X**	**X**	**X**
3 JULY	**X**	**X**	**X**
4 JULY	**X**	-	-
9 JULY	**X**	**X**	**X**
13 JULY	**X**	**X**	**X**
18 JULY	**X**	-	**X**
22 JULY	**X**	**No Data**	**X**
23 JULY	**X**	**X**	**X**
29 JULY	**X**	**No Data**	**No Data**
3 AUGUST	**X**	**X**	**X**
5 AUGUST	**X**	**X**	**No Data**
10 AUGUST	**X**	**X**	**X**
11 AUGUST	**X**	**X**	**X**
12 AUGUST	**X**	**X**	**X**
13 AUGUST	**X**	**X**	**X**
14 AUGUST	**X**	**X**	**X**

X – Indicates LLJ present

The spatial extents of the LLJ and the surface scalar flux have not been adequately documented and will become the focus of future studies. The variability in the time of maximum wind speeds is not well understood, and models do not capture it adequately. Studies to determine the horizontal structure of the LLJ are important because LLJ's have the capability to transport precursors, pollutants and particulates over hundreds of kilometers during the night. Since LLJ's have been observed on nights prior to many of the high pollution episodes, delineation of the horizontal structure will enable

us to determine how far ozone and other precursors can be transported. This may be a factor necessary to enable us to predict high ozone and other particulate matter episodes reliably.

CHAPTER 4

TRANSPORT BY LOW-LEVEL JETS AND THEIR IMPACT ON THE LOCAL METEOROLOGY

4.1 North-East Oxidant and Particle Study (NE-OPS)

The EPA-sponsored NEOPS campaigns (1998, 1999 and 2001), and Pennsylvania DEP-sponsored NEOPS (2002) campaign were conducted at a site prepared about 18 km northeast of Philadelphia. The primary objectives of the NE-OPS campaigns are to investigate the urban polluted atmosphere to find the relationships among conditions leading to high ozone concentrations and increased level of fine particles, determine the contributions from local and distant sources, and to examine the role that meteorological properties play in the build-up and distribution of pollutant concentrations. The program includes the instruments that are most useful for describing the evolution of air pollution events and examining the controlling factors of local meteorology on the particulate matter and chemical species distribution in the lower atmosphere. The NE-OPS campaigns are expected to improve our capabilities to forecast pollution events in the mid-Atlantic region, by providing an improved understanding of the influence of the local and regional dynamics and transport on the conditions that lead to the generation of air pollution episodes. The data obtained will help us to address the following questions.

- ?? Is the LLJ a major transport mechanism during ozone episodes?
- ?? How far can the nocturnal jet transport ozone and precursors?
- ?? How do ozone layers aloft affect surface concentrations?
- ?? Are LLJ's an important factor in air-pollution episodes?

4.2 Transport by Low-Level Jets

Mesoscale systems such as LLJ's have a profound effect on the transport and diffusion of pollutants in the boundary layer. Since most air pollutants from natural and anthropogenic sources are initially emitted within the planetary boundary layer, their short-range transport is usually determined by the mean wind distribution and turbulence within the boundary layer. The average speeds and directions of the pollutant transport are determined by the wind characteristics at the different heights. These pollutants eventually mix through out the boundary layer as they are transported over great distances by large-scale motions and systems. During nighttime, when the air is very stable, with the coldest air at the ground and the temperature increasing with height, the pollutants emitted from high stacks may accumulate in a thin layer above the ground.

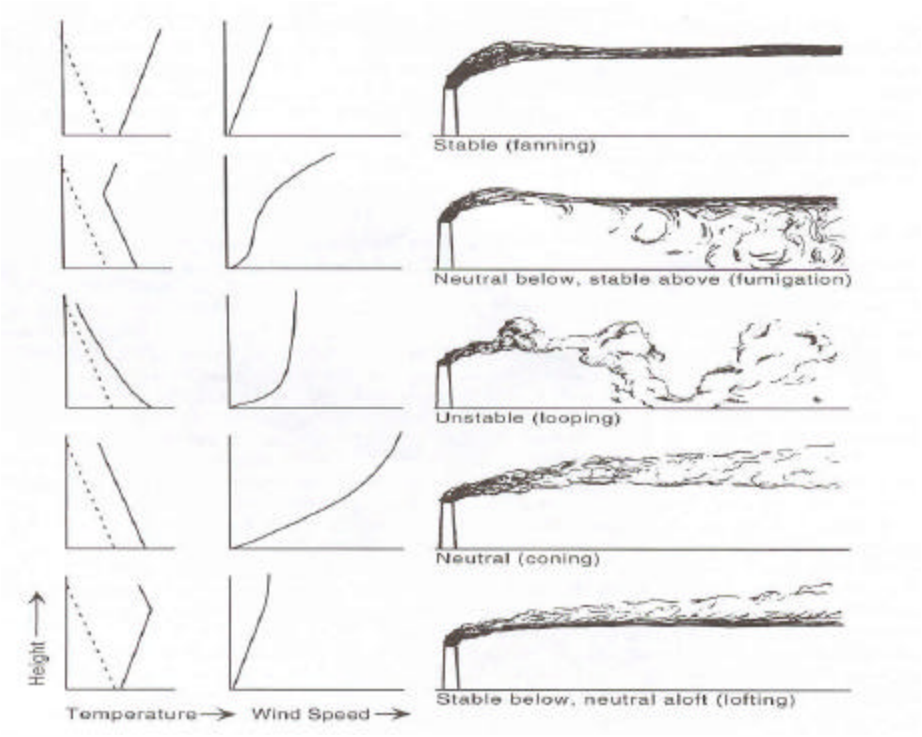

Figure 4.1 Schematic depictions of plume patterns in the boundary layer where the adiabatic temperature lapse rate is shown as a dotted line [Arya, 1999].

The patterns of the transported plumes for different wind speeds and temperature profiles are shown schematically in Figure 4.1. The processes of fanning and lofting are very important when considering the transport due to LLJ's, because they occur typically at night in a very stable boundary layer with strong surface inversion. They prevent the material from diffusing downward and concentrate it into a thin layer at the top of the inversion [Arya, 1999]. At sunrise, as the surface gets heated and convective mixing begins, this trapped layer of pollutants mixes down to the surface increasing the ground level concentration. Figure 4.2 illustrates the trapping of the pollutants in the night and the mixing process as solar heating begins.

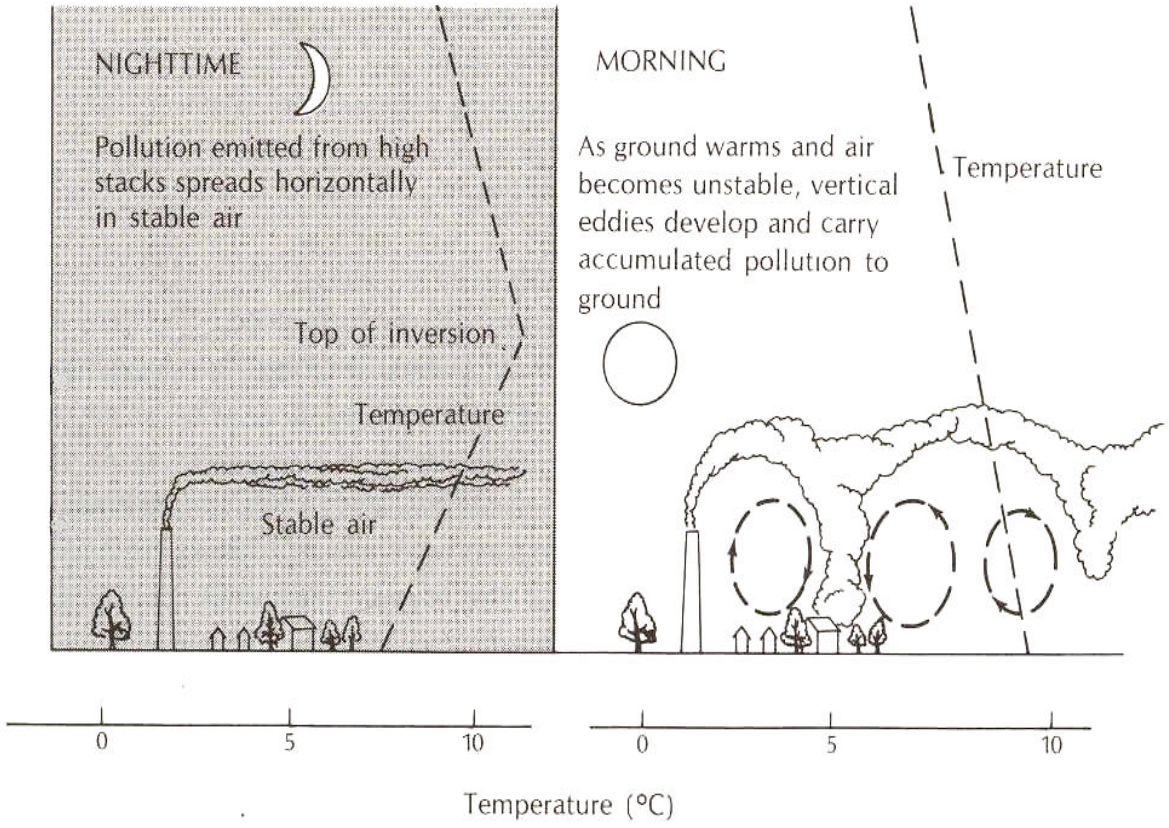

Figure 4.2 Illustration of the process of trapping of pollutants at nighttime and mixing during the day [Anthes et. al, 1975].

In the northeastern United States it has been seen that ozone concentrations are not only a product of urban-scale and mesoscale production of ozone, but are also influenced by the transport of ozone and precursors from the Midwestern and southeastern United States over distances that exceed 1000 km and on a timescale of one or more days [Wolff et. al, 1977, Willistford et. al, 2003]. Atmospheric conditions are generally more favorable for high ozone production during the summer months. Favorable synoptic-scale conditions leading to high ozone concentrations are associated with the quasi-stationary maritime tropical air masses, including light winds, high temperatures, few clouds and sparse rainfall [Seaman et al, 1998]. Seaman and Michelson analyzed the meteorological structures that contributed to high concentrations of ozone over the northeast region. Figure 4.3 explains this conceptual model schematically. They explained that as the Bermuda high moves northward over the mid-Atlantic region, south-southwesterly winds develop which favor accumulation of emissions over the region. Also, the sinking motion behind the Appalachian lee trough leads to lower altitude accumulation of emissions and the mixing depth variations across the trough favors less dilution of primary and secondary pollutants on the east of the trough. As the westerly flow behind the trough converges with the south-southwesterly flow ahead of it, an elevated mixed layer develops. These structures can lead to injection of boundary layer pollutants into the elevated mixed layer. Pollutants trapped in the elevated mixed layer are isolated from surface deposition, while the development of the nocturnal LLJ leads to rapid, long-range transport. The jets have the capability to transport ozone concentrations at night from upwind urban plumes into other regions and substantially contribute to the local production the following day. Often the highest concentrations of

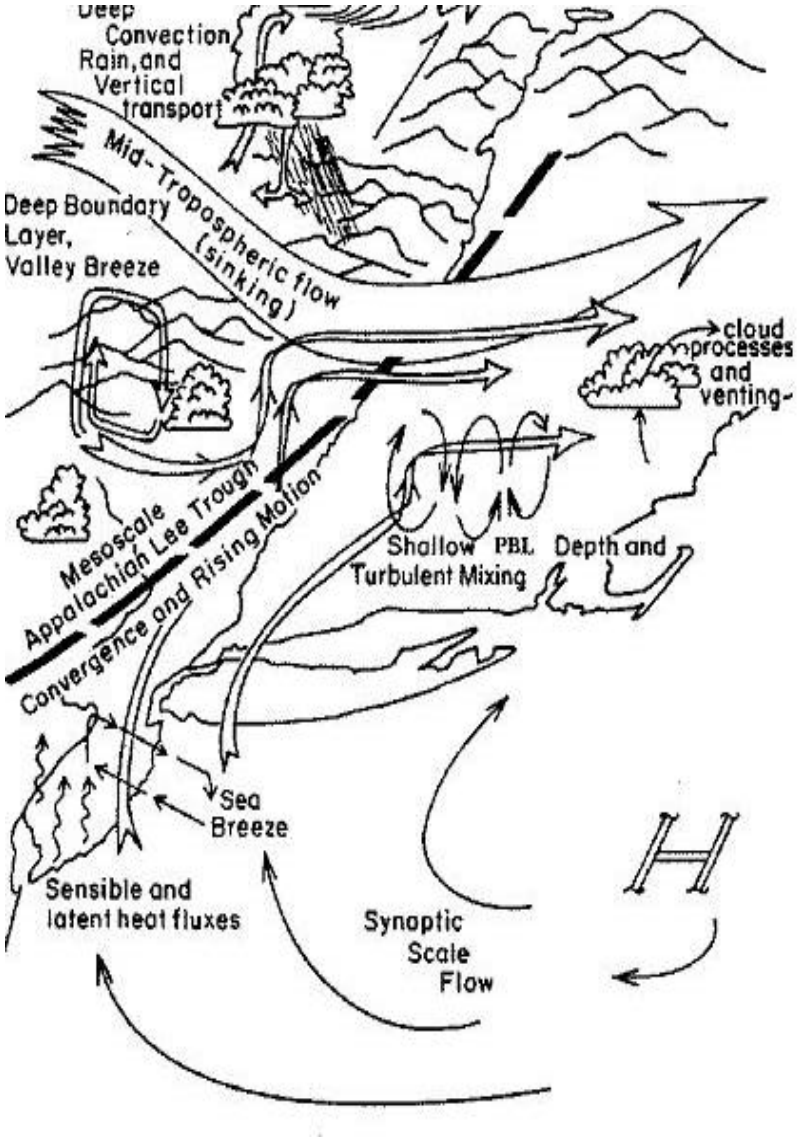

Figure 4.3 Schematic showing the conceptual model of the meteorological structure during high-ozone episodes in the Northeast region [Seaman et al, 1998].

ozone during a multi-day episode is reported during the afternoon following a well-developed nocturnal jet. In addition, a rapid increase in ozone concentrations that is sometimes observed in the early morning hours can be attributed to the vertical transport of ozone during "bursting" episodes, which occur due to dynamic instabilities in the shear layer between the surface and the layer of maximum wind speed [Clark et al, 2001]. In

1997, Blumenthal et al showed that during the NARSTO 1995 study, low-level jets occurred on six out of nine nights preceding a regional ozone episode day [Blumenthal et. al, 1997]. They also indicated that low-level jets were two to three times more likely to be observed on nights preceding ozone episode days than on other nights. We have been able to extend those analyses and determine the role that LLJ's play in the generation of high pollutant concentrations at Philadelphia using the larger data set now available from the NEOPS program.

4.3 Results from NEOPS

Measurements obtained from the NARSTO-NEOPS investigations in Philadelphia during the summers of 1999 and 2002 document the influence that low-level jets have on modifying the properties of the residual boundary layer. Several periods show meteorological control and transport of air mass in the results obtained from the various instruments used in the studies.

4.3.a NEOPS Campaign – 1999

Summer 1999 was considerably warmer and drier than normal with temperature in the 90^{th} percentile and precipitation in the 10^{th} percentile relative to the 1895-1998 long-term average [Clark et al, 2001, Ryan et al, 2001]. The 500 hPa ridge over the mid-Atlantic region and surface high pressure centered over the Carolinas dominated the weather conditions. Table 4.1 provides a brief description of the episodes documented during the study in 1999. Figure 4.4 shows the ozone concentration during the 1999 campaign and indicates the days when low-level jets were present. During the summer of

1999, low-level jets were observed on nights prior to five out of the six high ozone episodes in Philadelphia and occurred on 4 out of 5 days when ozone concentrations exceeded 100 ppbv.

Table 4.1 1999 NE-OPS Episodes [Clark, 2001].

Date	Description of Episode
Jul 3-5	Warm Sector, high temps (37.2C), strong low level wind, Code Orange O_3
Jul 8-10	Frontal Passage 7/8, warm sector 7/9 with strong 850 h Pa advection. Moderate wind, Code Yellow O_3 with Code Orange west of site.
Jul 15-20	Strongest O_3 episode of season. Ramp-up and recirculation event followed by stagnation. Weak W to SW wind with strong Bermuda High. Many (17) 1-hour exceedances on 7/19. Ramp-up [$PM_{2.5}$]. SW LLJ's evident during 16-19 July.
Jul 23-24	Recirculation late 7/22 followed by SW 12 ms^{-1} wind and Code Orange O_3. Upper level ridge brings warm 850 hPa temps. TRW's end the episode on 7/24.
Jul28-Aug1	Lower 0_3 levels 7/28-7/30 with W wind followed by lee trough on 7/31, SW wind, spike of 165 ppbv O_3 and passage of sea breeze front. Mobile trough on 8/1 ends the episode. High [$PM_{2.5}$] correlate with low [O_3].
Aug 4-5	High O_3 levels distributed by frontal passage, NW 12 ms^{-1} winds and low T_d keep O_3 in Code Orange. Reduced temps.
Aug 11-13	Warm sector, recirculation of high O_3 before passage of bay breeze, strong bay breeze on 8/12 cleanses.
Aug 16-17	Similar meteorology to Aug 11-13 with spike in O_3 on 8/17.

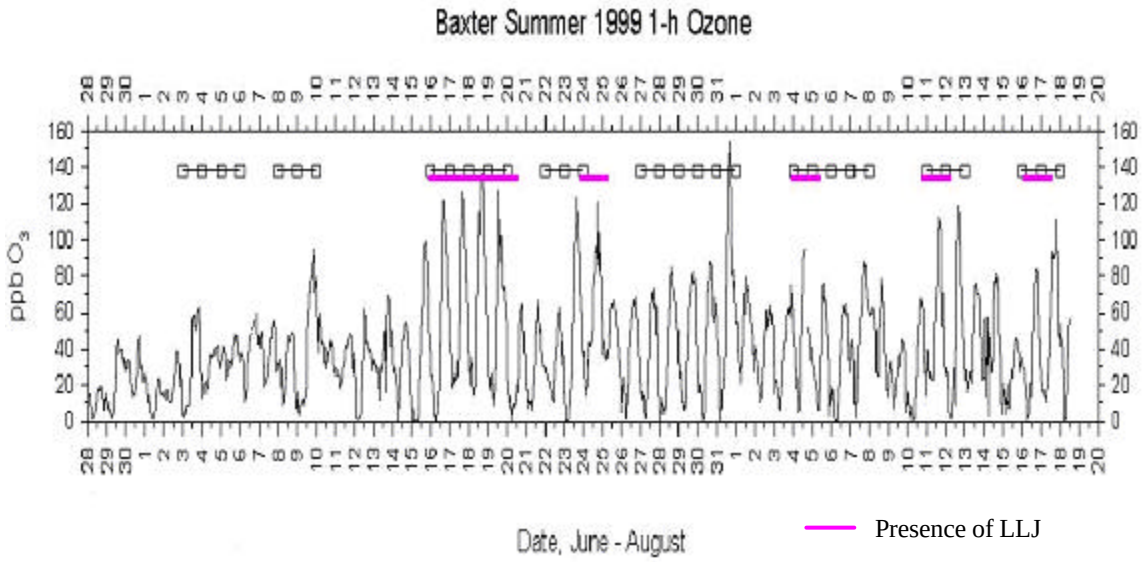

Figure 4.4 Surface ozone concentrations of 28 June- 20 August 1999.

The summer's strongest and longest ozone episode occurred during the period from 15 to 19 July. High temperatures, strong short-wave radiation, and westerly flow dominated the mid-Atlantic and northeastern U.S region; these conditions are favorable for the transport of pollutants from the mid-west to the East and for the formation of ozone and other pollutants [Zhang et al, 2001]. During this period, ozone and other pollutant concentrations increased rapidly to very high levels, which suggest that local sources were not the sole contributors. Without transport into the region, it would be unlikely that local sources would be able to produce ozone that quickly, and at such high concentrations. A low-level jet is seen in the profiler data on 16 July 1999, and we hypothesize that this jet contributed to the episode by transporting pollutants and other precursors into the Philadelphia region. The sequences of plots that follow depict the influence that low-level jets had on the air pollution episode that took place during this period in Philadelphia. LLJ's were present on all nights between 16 and 19 July with

wind speeds reaching 15 ms^{-1}. At these speeds the LLJ can transport parcels over 200 km during the night. Figure 4.6 shows the LLJ's present during the 15 – 19 July episode. The LLJ is present at its characteristic height between 400-800 m and dies out near sunrise when solar heating erodes the wind field. The LLJ was seen to grow in intensity as the episode matured and diminished on 19 July when a cold front approached. Back-trajectories in Figure 4.5 obtained from NOAA show that the trajectories of air parcels reaching the site at 0600 UTC, at the height of the LLJ, are transported from the southwestern/western boundary. The potential for pollutant transport from the west by low-level jets during nighttime is seen in the back trajectories and wind profiler data. We hypothesize that these air parcels being transported from the western boundary into the Philadelphia region by the jet contain a reservoir of ozone and pollutant precursors. When convective mixing begins the following morning, these transported materials are mixed to

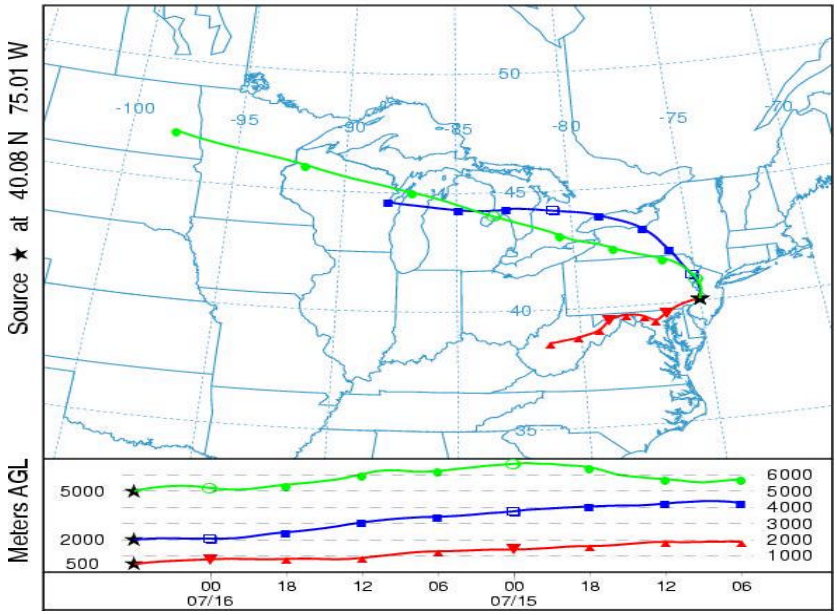

Figure 4.5 Back trajectories ending at 6 UTC on 7/16/99 (www.arl.noaa.gov/ready.html).

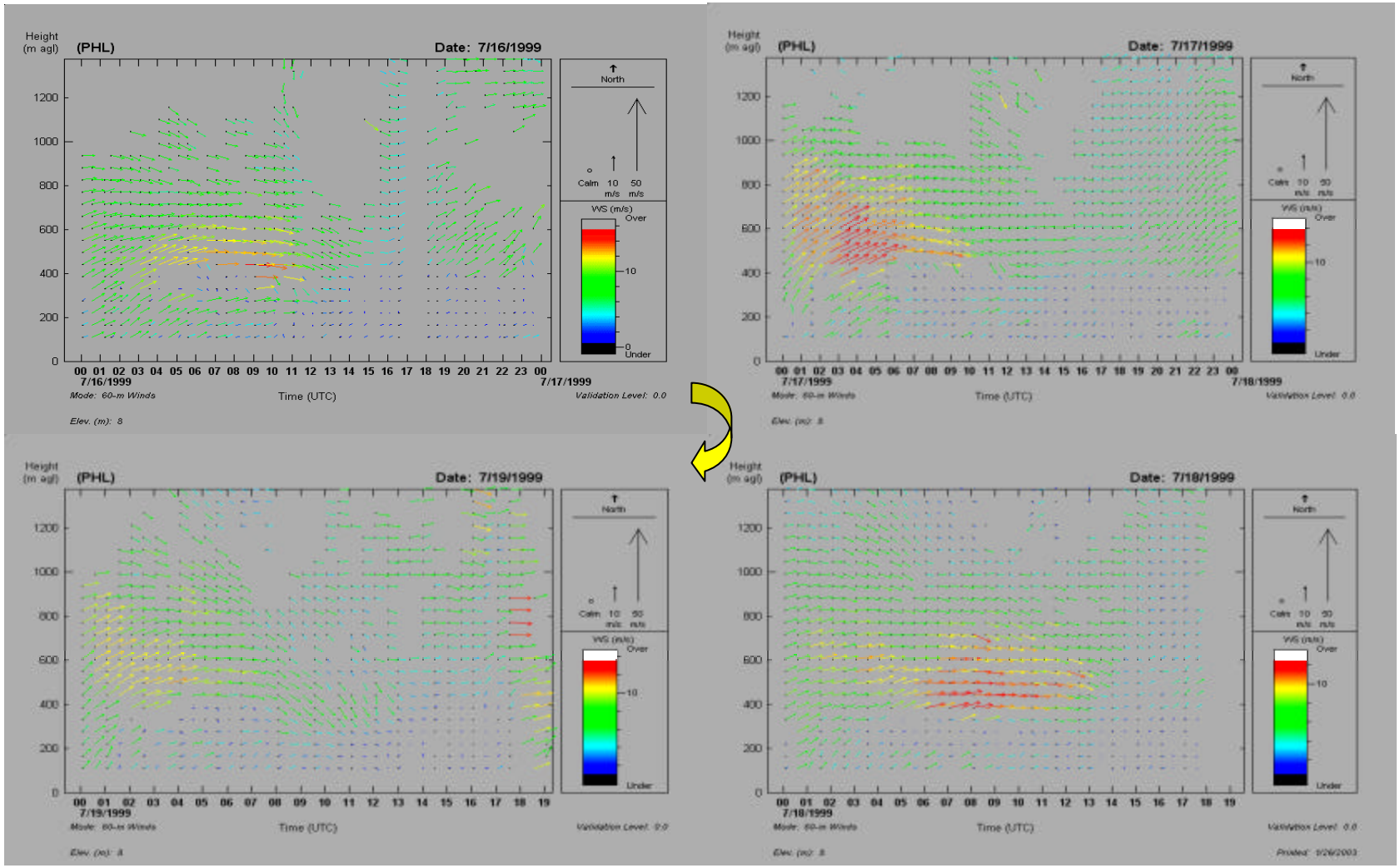

Figure 4.6 Presence of LLJ's during the July 15th – 19th 1999 high ozone episode.

the surface and become available to freely react and form ozone. These transported materials also mix to the surface during "bursting" events, which are seen to occur in the early morning hours from mechanical instabilities in the shear zones below the layer of maximum winds. These bursting events vertically mix the pollutant and precursor concentrations, being advected aloft by the low-level jet, to the surface. Figure 4.7 shows the effect of these bursting events on the surface ozone concentrations. It is seen that the surface ozone concentrations increase by about 10-20 ppbv within a few minutes during the early morning hours on each day of the episode. It is unlikely that local sources would be able to produce such high concentrations of ozone that quickly. Hence, the concentration of materials being brought in by the jet, that are mixed down during these bursting events, must definitely contain ozone or chemical species that can decompose to form ozone without photochemical processes at night. These bursting events are also important because some of the ozone precursors mixed to the surface may remain

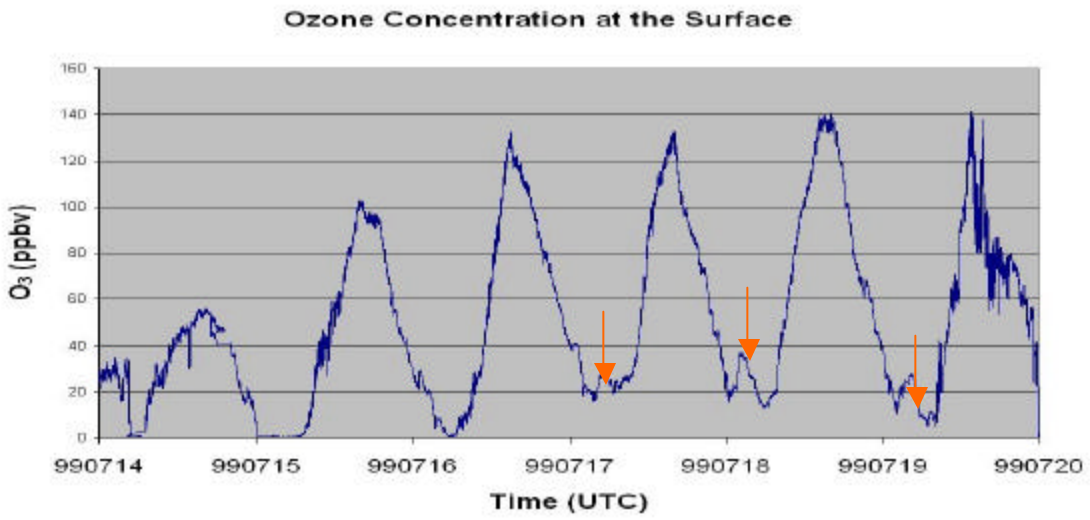

Figure 4.7 Surface ozone concentrations for the 15-19 July 1999 episode (Clark, Millersville University).

dormant in the surface layer through the night. As the sun rises and convective mixing begins, these precursors may freely react to form ozone and other pollutants. We hypothesize that this could be a reason for the quick increase in ozone levels once surface heating begins, as local sources acting alone will not be able to produce such high levels of ozone as rapidly. Figure 4.8 shows the signature of the nocturnal jet in the water vapor mixing ratio during the pollution episode. Water vapor profiles provide valuable information about short-term kinematic processes in the planetary boundary layer and also serve as a tracer for transport of atmospheric constituents. A clear picture of the aloft air mass can be seen moving in time at a height of about 500 m. The height of the dry layer, containing lower humidity continental air, coincides exactly with the height of the

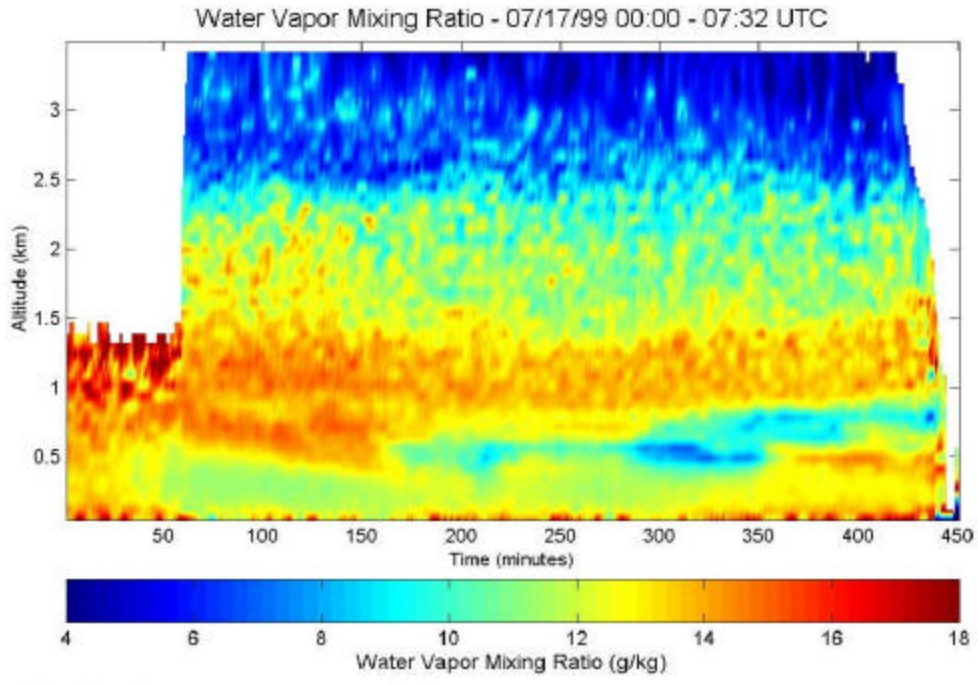

Figure 4.8 Water vapor mixing ratio from PSU Raman lidar shows dry layer at 500 m caused by the LLJ.

jet. The dry layer is due to dry continental air being advected from the west by the jet. We hypothesize that this plume of dry air transported ozone and other pollutant precursors, which dissociated in warmer temperatures at the surface to quickly produce the high ozone concentrations. The surface concentrations of PM2.5, sulfate, black carbon and SO_2 obtained from 12 July to 26 July at Philadelphia are shown in Figure 4.9 and they also indicate the contribution of the jet. The concentrations of PM2.5 and sulfate are seen to increase by about 20 ?g/m^3 within a few hours. These concentrations are twice as high as on the days when there was no transport into the region. This indicates that PM2.5, sulfate, and other pollutants were transported into the region during the night, and the low-level jet was a contributor to the process. The concentrations of PM2.5, sulfate, SO_2 and black carbon, shown in Figure 4.9, are seen to increase rapidly when the stable boundary layer begins to disintegrate and mixing begins to bring the pollutants and precursors down to the surface. For the surface concentration levels to increase as rapidly as they did, the concentration of pollutants and precursors in the aloft reservoir must be high. The concentrations of pollutants were observed to be much higher on days following the low-level jet. The sudden increase in concentration of pollutants seen after the bursting events and when the mixed layer begins to form indicate that the pollutants and precursors being advected along by the jet do play a vital role in the generation of the pollution episodes observed in 1999.

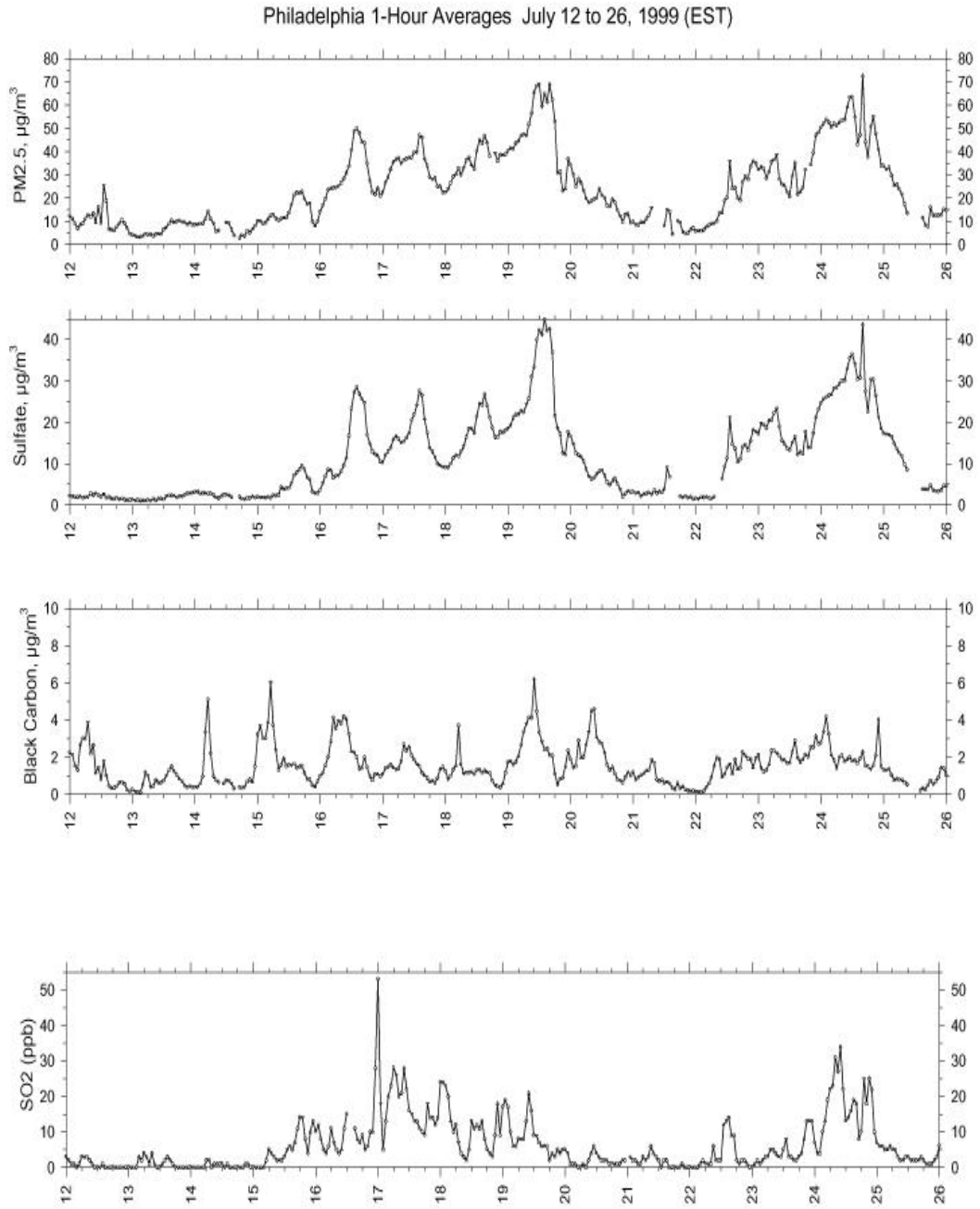

Figure 4.9 One-hour averages of PM2.5, Sulfate, Black Carbon and SO_2 (Allen, Harvard School of Public Health).

4.3.b NEOPS-DEP Campaign – 2002

The summer of 2002 was warm and dry, particularly during the NEOPS intensive operation period (late June – early August). During this period, 22 days (~50%) reached or exceeded 90? F (Ryan et al, 2003). For most of the mid-Atlantic, temperatures were in the 90th percentile, and precipitation amounts were variable but consistently below normal. While the Bermuda high was located at no higher latitude than normal, high pressure was observed to extend further north and west than usual. With conditions favorable to ozone formation and transport, ozone concentrations were observed to rise beyond 100 ppb on a few days. Table 4.2 gives a description of the events documented during the NEOPS 2002 campaign, which were accompanied by LLJ's. As with the summer of 1999, low-level jets were observed on most nights prior to mid-day ozone concentrations exceeding 100 ppbv. Figure 4.10 shows the ozone concentrations measured at the surface during the 2002 campaign.

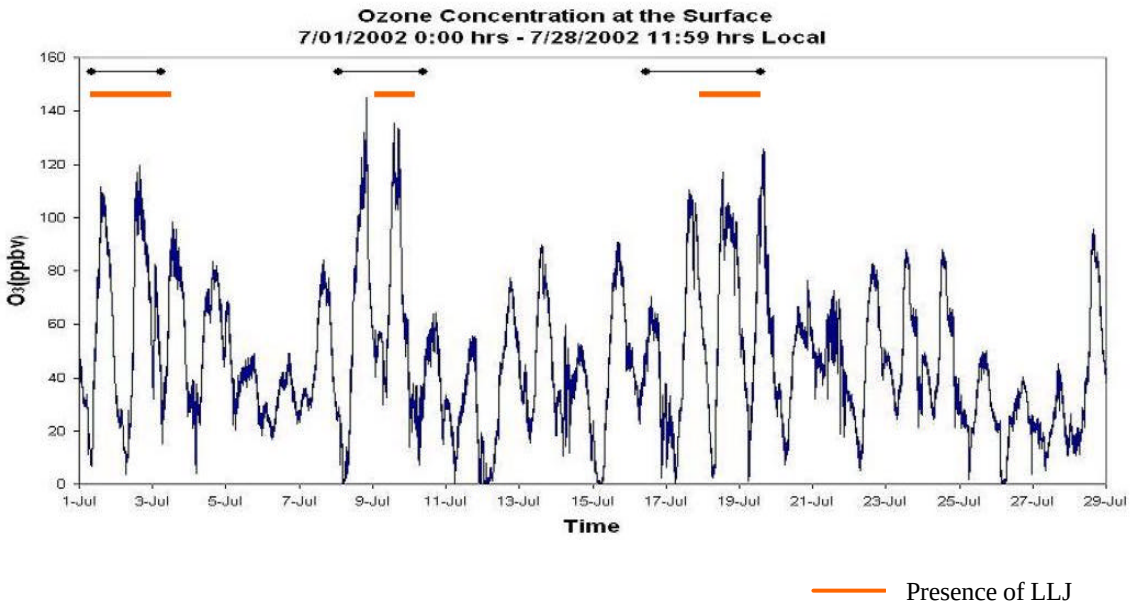

Figure 4.10 Surface ozone concentrations observed at Philadelphia during July 2002.

Table 4.2 2002 NEOPS episodes.

Date	Description of Episode
Jul 1-4	LLJ's were evident with wind speed's reaching 14 ms^{-1} between 400-800m during the early hours of the night in the SW direction. High Ozone episode with O_3> 100 ppbv.
Jul 7-9	Highest ozone period of the campaign with ozone touching 140 ppbv. Strong LLJ's were observed during the nights. (Canadian wild fires)
Jul 11-13	Strong Nocturnal jets accompanied with a high ozone (90 ppbv) episode.
Jul 22-24	High ozone concentrations with presence of Nocturnal jets.
Aug 8-11	Characteristic nocturnal jets are observed with wind speeds of 15 ms^{-1}

The episode of July 1 to 4, 2002 included periods with peak ozone reaching 120 ppbv on 2 July. Back trajectories and regional surface observations during the episode suggested that the transport of pollutants was from west to east. The back trajectories in Figure 4.11 show that air parcel trajectories shifted from a recirculation along the northeast corridor to a westerly flow as the episode matured. We hypothesize that the presence of low-level jets during the episode played an important role in contributing pollutants and precursors from the western boundary into Philadelphia. A sequence of plots follow that show the transport capability of the jet and the impact of the transported materials on the local meteorology. Figure 4.12 shows the co-location of the aloft ozone with the low-level jet in time sequences obtained with the Penn State Raman lidar. The plume that is being transported by the jet could be a reservoir for ozone, ozone precursors

and other pollutants. The jet on 2 July, which had peak speeds of 15 ms^{-1} and lasted for over 5 hours, could have transported materials from regions 250 km away into Philadelphia during the night. The back trajectories show the air parcels brought into the site by the jet to be from the western boundary. The time sequence of ozone clearly shows the mixing of the aloft ozone concentrations to the surface when the mixed layer begins to form and the boundary layer rises to the height of the plume. As the plume

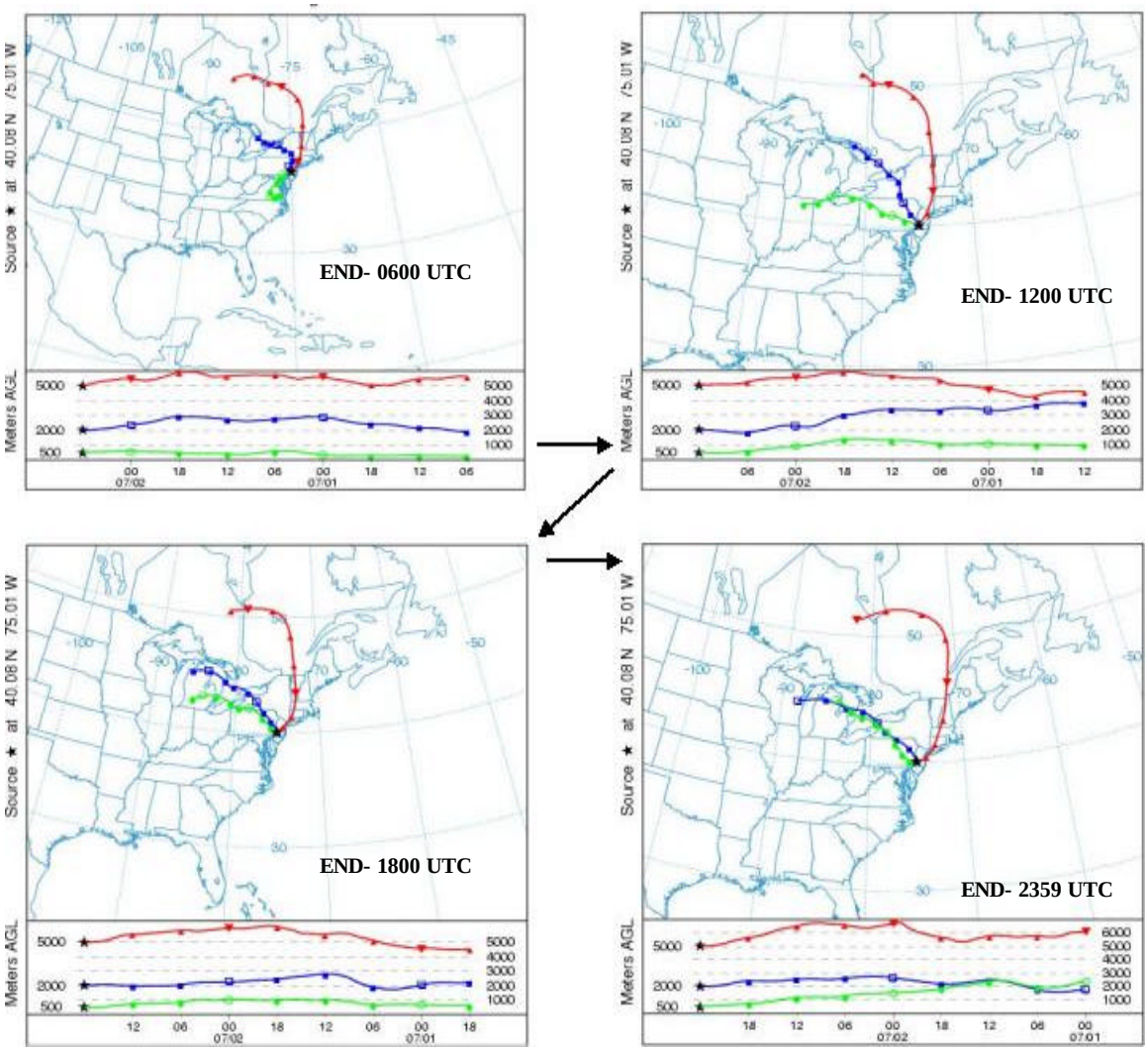

Figure 4.11 Back trajectories for 7/02/2002 indicating westerly transport into the northeast region (www.arl.noaa.gov/ready.html).

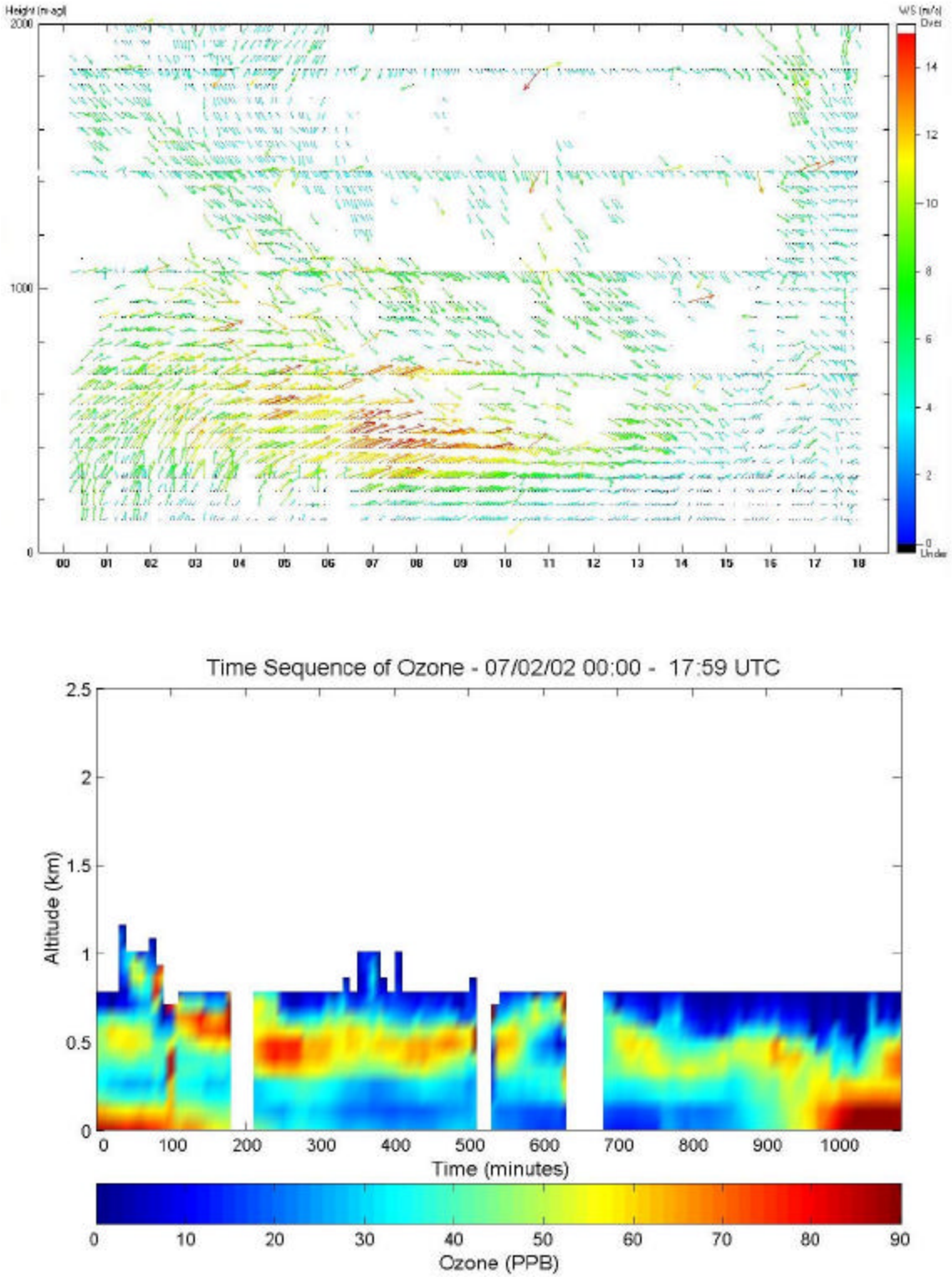

Figure 4.12 Low-level jet and ozone aloft over Philadelphia on July 2 2002.

mixes to the surface, warm temperatures at the surface aid in thermal decomposition of the precursors, which quickly produce high ozone concentrations by photochemical processing of the transported materials. It is hypothesized that the transport reservoir might contain peroxyacetyl nitrate (PAN), which quickly dissociates into ozone precursors at temperatures near 30?C. In the absence of transport from outside of the region it is unlikely that local sources would be able to produce ozone at such high concentrations. The effect of the low-level jet was also seen to increase concentrations of NO_X, SO_2, and $PM_{2.5}$. Their concentrations increased to levels much higher than days when conditions were not favorable for transport into the region. Figure 4.13 and Figure 4.14 show the concentrations of ozone and NO_X/NO/NO_2 on July 2 2002. Since photochemical reactions do not occur at night, we hypothesize that the sudden increase in NO_X/NO/NO_2 concentrations seen at 0300 EDT is due to the mixing from the aloft transport reservoir to the surface during a bursting event caused by the wind shear. Nitric oxide, NO, is an important primary pollutant emitted by both automobile and stationary sources. Small quantities of nitrogen dioxide, NO_2, are also emitted along with NO. NO is converted in ambient air to NO_2. Thus NO_2 is both a primary and a secondary pollutant. The primary pollutant NO_x (mainly NO) reacts in the presence of non-methane hydrocarbons and sunlight to form a host of secondary pollutants such as ozone. In the early morning hours, the concentrations of NO rise and reach a maximum at a time that approximately coincides with the peak automobile traffic. Subsequently, we see a maximum in the concentrations of NO_2. At 0630 EDT we see that the excess NO concentrations produced from traffic acts to reduce the ozone concentrations. Ozone, which is relatively low in the early morning, increases significantly about noon when the

NO concentrations drop to a low value as photochemistry uses the NO_x to generate ozone. Ozone reaches a maximum after NO_2 decreases, because its effect is to initially cause loss of ozone by photolysis but photochemistry later acts on it to produce ozone. Since NO reacts relatively rapidly with ozone to form NO_2, significant concentrations of ozone and NO cannot co-exist. This is the reason why ozone peaks only after NO has fallen to very low concentrations. As solar heating began, the increase in ozone concentrations caused the NO_X levels to decrease at the surface as it contributed to the

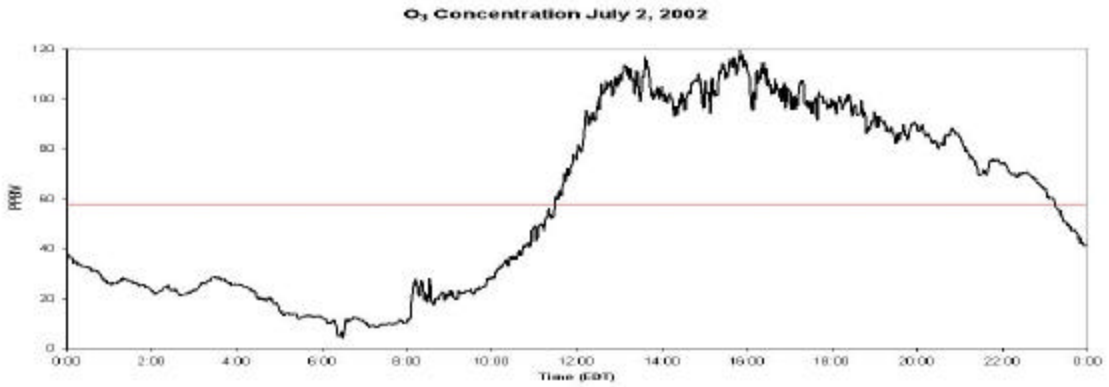

Figure 4.13 Surface ozone concentrations on July 2 2002 (Clark, Millersville University).

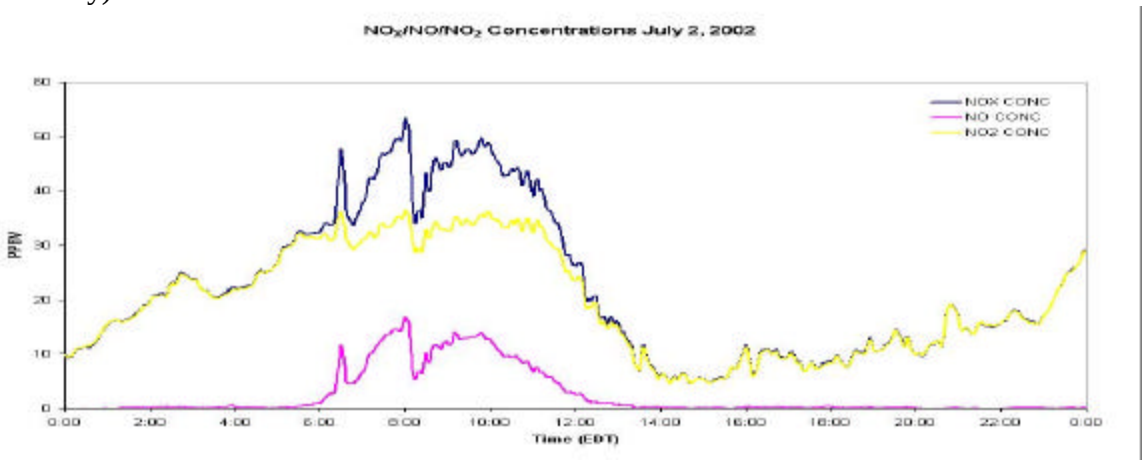

Figure 4.14 Surface $NO_X/NO/NO_2$ concentrations on July 2 2002 (Clark, Millersville University).

photochemical production of ozone. The relationship that exists between ozone and NO_X/NO/NO_2 concentrations is clearly portrayed in Figure 4.13 and Figure 4.14. During the summer of 2002, the concentrations of NO_X/NO/NO_2 were observed to be much higher on days following low-level jets. This implies that the precursors and pollutants transported by the jet during the night play a significant role in increasing pollutant concentrations at the surface the following day. The spike in the surface ozone concentration at around 0800 EDT is due to a bursting event that mixed the ozone from the storage/transport layer to the surface. Ozone concentrations are seen to increase by about 20 ppbv within a few minutes. The added concentrations that are mixed to the surface from the transport reservoir could be a primary cause for the very high concentrations observed. The effect of transport into the region by low-level jets also correlates with the increase in concentration levels of SO_2, $PM_{2.5}$, and black carbon. The significant increase in the concentrations of SO_2, $PM_{2.5}$ and black carbon are shown in Figure 4.15 and Figure 4.18.

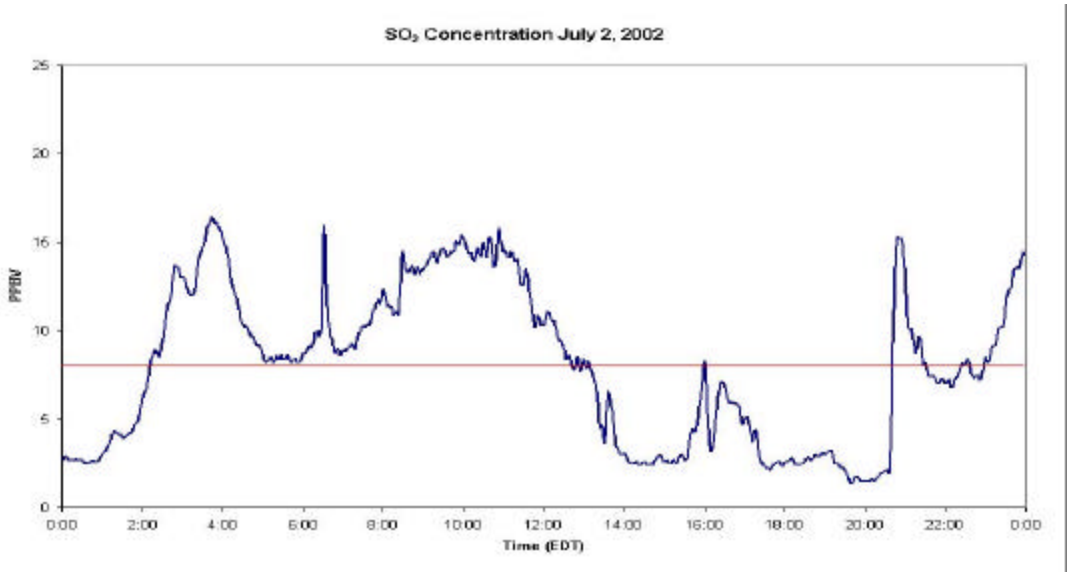

Figure 4.15 Surface SO_2 concentrations on July 2 2002 (Clark, Millersville University).

The effect of transport in to the Philadelphia region was also evident in the surface concentrations and time sequences of ozone on 3 July 2002. Ozone concentrations at the surface were observed to increase to 80 ppbv during the night. The time sequence of the Raman lidar clearly shows transport into the region by the low-level jet and the mixing down of the transport reservoir to the surface during a bursting event. The mixing down occurred at the time when surface concentrations were seen to increase

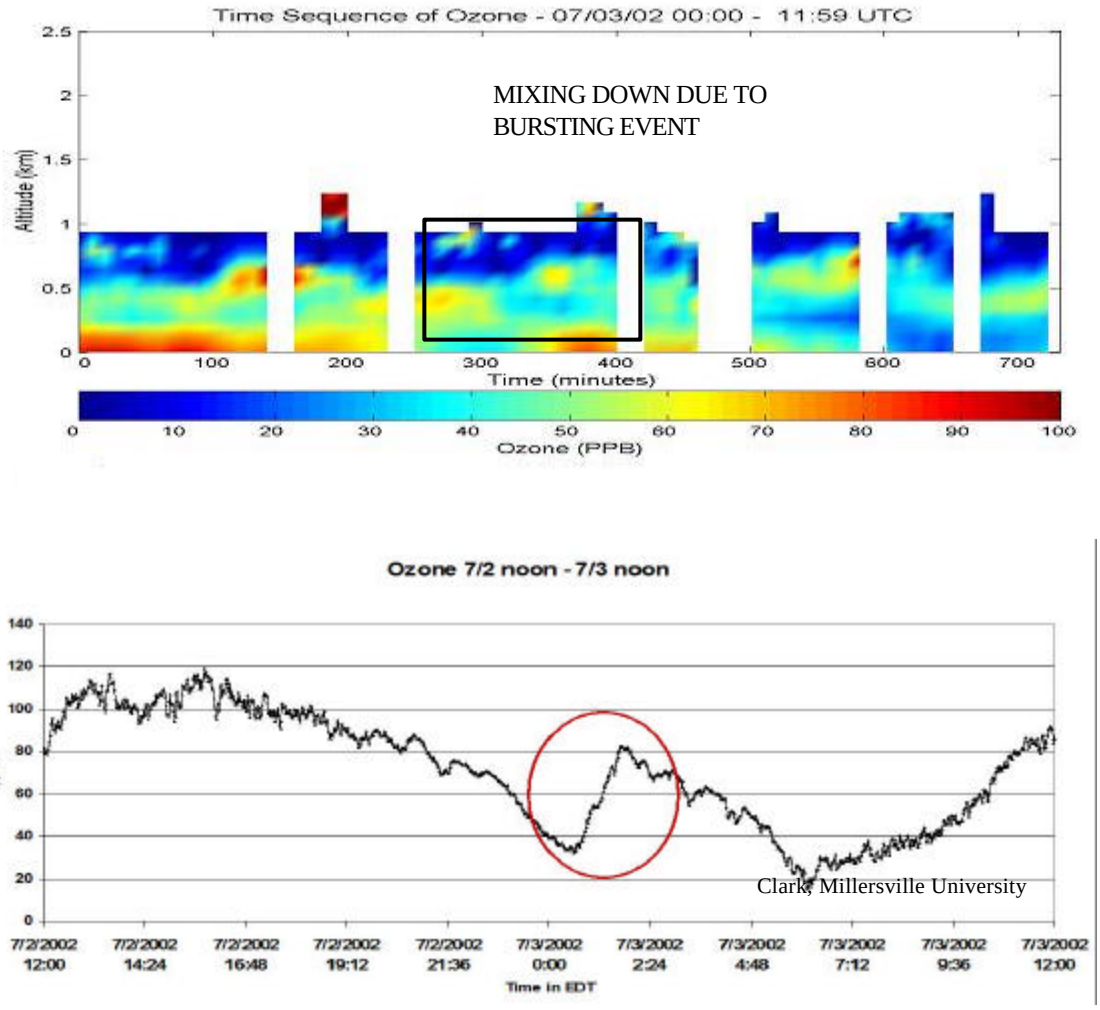

Figure 4.16 Increase in surface concentrations of ozone due to mixing from the region aloft.

rapidly. Figure 4.16 shows the effect of the mixing down of the plume aloft on the surface concentrations. The concentrations of PM2.5 and black carbon were also seen to increase due to the mixing from aloft.

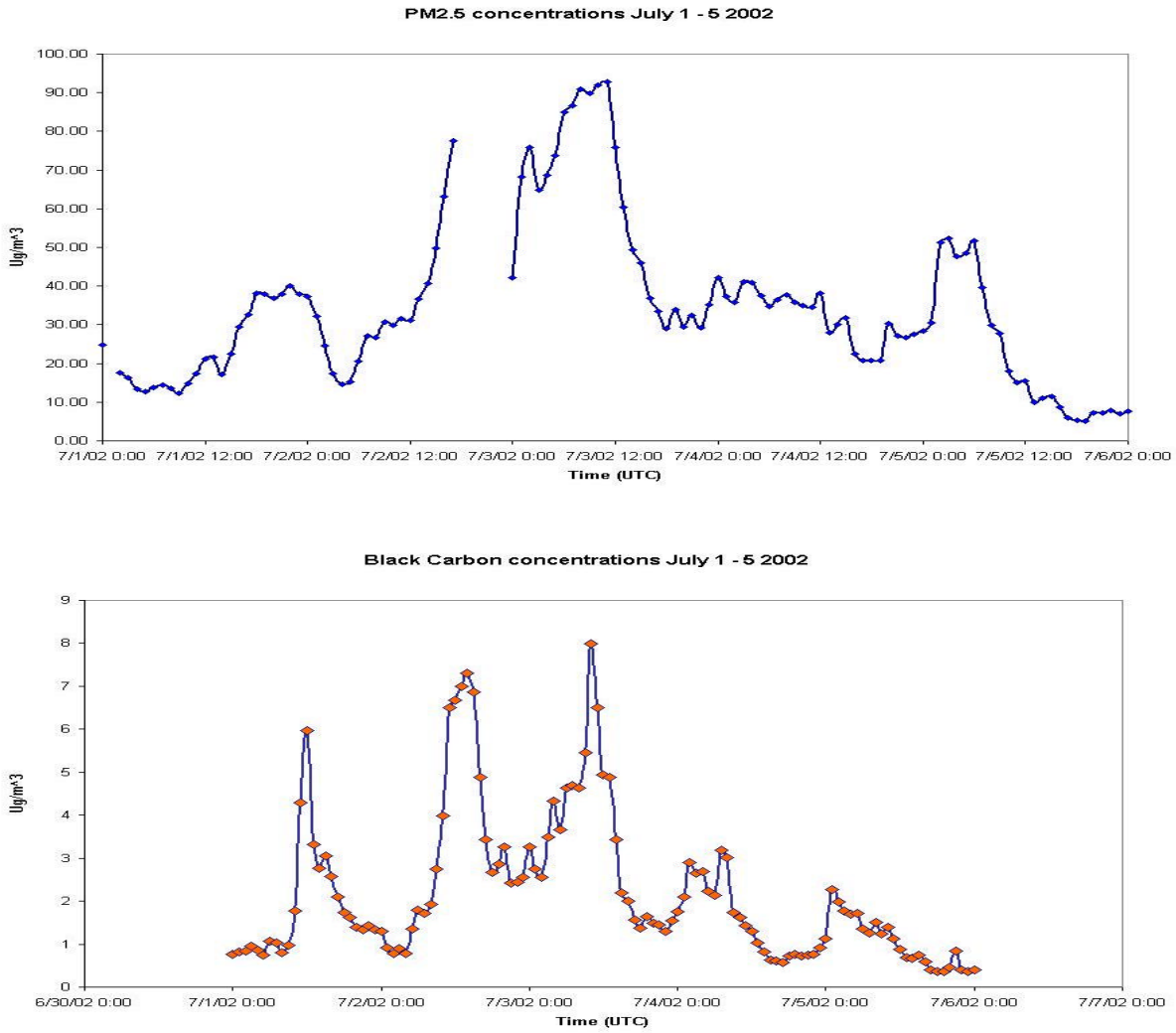

Figure 4.17 PM2.5 and black carbon plots during the July 1 – 4 episode (Hopke, Clarkson University).

Low-level jets, which enhanced the local production by transporting pollutants into the region, accompanied most of the high ozone episodes that occurred during the summer of 2002. The concentration of SO_2, PM2.5, black carbon and NO_X/NO/NO_2 all

showed significant increases as the jet transported pollutants and precursor material in to the region. All the episodes were associated with transport into the region and were accompanied by increases in pollutant concentrations as described in the July 1 to 5 episode. Table 4.3 shows the concentrations of pollutants observed at the surface following the occurrence of low-level jets. The resulting background concentrations are a mixture of ozone transported from different locations as the wind oscillates and changes its direction. The impact of the concentrations aloft, being advected along by the jet, plays a vital role in the generation of the high pollutant concentrations at the surface. This suggests that the jet acts as an important transport mechanism and is not just a meteorological artifact.

Table 4.3 Pollutant concentrations at the surface following LLJ's in July 2002.

Low Level Jet Date	Sulfur Dioxide PPB > 15	Nitric Oxides PPB > 40	Ozone PPB > 80
7/01/2002	X	X	X
7/02/2002	X	X	X
7/03/2002	X	X	X
7/04/2002	X	X	X
7/09/2002	X	X	X
7/13/2002	13PPB	30PPB	X
7/18/2002	13PPB	X	X
7/23/2002	X	X	X
7/29/2002	No Data	X	X

The measurements obtained during the NEOPS campaigns provide valuable information on the processes that control the generation of high ozone pollution episodes in the northeast region. The database documents the characteristic features of the of the northeastern low-level jet and has proven to be a starting point for determining the role that the nocturnal jet plays in the generation of air pollution episodes in the northeast region

CHAPTER 5

CONCLUSIONS

Data obtained during the NE-OPS summer campaigns of 1999, 2001 and 2002 have been analyzed and they document the presence of low-level jets over the northeastern United States. Such jets have been observed and studied extensively over the central United States, but they are not as well understood in the northeastern United States. This database, along with measurements obtained at other sites such as the Rutgers University, NJ, and Fort Meade, MD, sounders have helped us to characterize certain features of the northeastern low-level jet and study the influence that these jets have on modifying the properties of the boundary layer. A few salient characteristics of the northeastern low-level jet, observed during the NEOPS campaigns, are summarized below;

- ?? They usually form under clear sky conditions in the presence of a quasi-stationary high-pressure system, which allows for maximal amount of differential heating and cooling between the eastern coastal plain and the Appalachian Ridge.
- ?? Northeast LLJ's exhibit the characteristic rotation of the wind field in time, which is an important factor when considering air pollution episodes because of its ability to change the trajectories of air parcels reaching the site from upstream locations.
- ?? They are usually confined to their characteristic region between 300-1000m.

- ?? Observed maximum wind speeds vary between 10-20 ms^{-1}. At these speeds the LLJ's have the capability to transport pollutants and precursors over distances of 250 km during the night.
- ?? Time of occurrence of the maximum wind speed is considerably variable but within the same hour at each of the examined sites.
- ?? LLJ's generally reside on top of the nocturnal inversion and are decoupled from the surface.
- ?? Bursting events, characteristic of LLJ's, occur due to the dynamic instability in the shear zones between the surface and the layer of maximum winds. They are important because they can vertically mix the transported plume to the surface and cause pollutant concentrations to increase rapidly during a period of a few minutes.
- ?? We define the northeast LLJ as one in which the maximum wind speed at the jet core should be at least 3 ms^{-1} greater than the region above and below the core. Also, it should be the first wind maximum occurring above the surface and below the altitude of 1200 m. Future analysis of LLJ's along the east coast region will be based on a more stringent criteria for defining LLJ's.

Penn State's LAPS lidar and wind profiling Radar/RASS systems were used to study the characteristics of LLJ's and understand the role that LLJ's play in the generation of air pollution episodes. The signatures of the jets were also observed in Millersville University's surface trace gas analyzers, and Clarkson University's aethalometer and OC/EC instruments. Analysis of the data revealed that low-level jets

were present on 7 out of 8 nights prior to days when ozone concentrations exceeded 100 ppbv. The surface concentrations of other pollutants were also seen to be dramatically high on days following the low-level jet. Time sequences of ozone and water vapor clearly show concentrations of pollutants being advected along by the jet. These pollutants mix to the surface when the mixed layer begins to develop and during the bursting events. The transport reservoir that is mixed down has the effect of increasing the concentrations of the pollutants drastically. These sudden increases in pollutant concentrations are evident as spikes in the surface pollutants concentrations during the morning hours. Without transport into the region it is unlikely that local sources would be able to produce the observed ozone as quickly and at such high concentrations. It is hypothesized that the large quantities of ozone and pollutant precursor materials are transported into the region by the low-level jets and these play a vital role in the generation of the high concentrations of pollutants observed during the episodes. Measurements interpreted with the use of back trajectories also suggest that increased levels of pollutant and precursor transport occur when the jet becomes a conveyor of air parcels from the western boundary. The data obtained during the NEOPS campaigns show the capability of the low-level jet to transport pollutant and precursor materials over long distances during the night and cause a drastic increase in surface concentrations the following day. Hence, we suggest that the LLJ's act as an important transport mechanism and is not just a meteorological artifact.

Future studies to determine the type of pollutants being advected by the jet and the exact location from which these pollutants were transported will enable us to forecast air pollution episodes more effectively. It will also help us to develop systematic

approaches to tackle transport-induced episodes in regions where local sources do not contribute much to air pollution.

REFERENCES

Anthes, Richard A., Hans A. Panofsky, John J. Cahir, Albert Rango, The Atmosphere, Bell & Howell Company, Ohio, 1975.

Arya, S. Pal, Air Pollution Meteorology and Dispersion, Oxford University Press, Oxford, 1999.

Balsiger, Franz, Paul T. Haris, and C. Russell Philbrick, "Lower Tropospheric Temperature Measurements Using a Rotational Raman Lidar," Optical Instruments for Weather Forecasting, SPIE Vol. 2832, 53 – 60, 1996.

Banta, R. M., R. K. Newsom, J. K. Lundquist, Y. L. Pichugina, R. L. Coulter, L. D. Mahrt, "Nocturnal Low-Level Jet Characteristics Over Kansas during CASES-99," Bound. Layer Meteor., 105(2), 221 – 252, 2002.

Blackadar, A. K., "Boundary Layer Wind Maxima and Their Significance for the Growth of Nocturnal Inversions," Bull. Amer. Meteor. Soc., 38, 283 - 290, 1957.

Blumenthal, Donald L., Fredrick W. Lurnmann, Naresh Kumar, Timothy S. Dye, Scott E. Ray, Marcelo E. Korc, Richard Londergan, Gary Moore, " Transport and Mixing Phenomena Related to Ozone Exceedances in the Northeast U.S.," prepared for the Ozone Transport Assessment Group, 1997.

Bonner, William D., "Climatology of the Low-Level Jet," Monthly Weather Review, 96, 12, 833 – 850, 1968.

Chadha, Ginnipal S., " Optical Systems Design for ALAPS Lidar Instrument," Master of Science Thesis for Penn State University, Department of Electrical Engineering, May 2001.

Clark, R. D., C. R. Philbrick, W.F. Ryan, B.G. Doddridge, J. W. Stehr, "The Effects of Local and Regional Scale Circulations on Air-pollutants During NARSTO-NEOPS 1999-2001," 4th Conf. On Atmos. Chem., Amer. Meteor. Soc., 125-132, 2001.

Cooney, J. A., " Comparisons of Water Vapor Profiles Obtained by Radiosonde and Laser Backscatter," J. Appl. Meteor., 9, 182 – 184, 1970.

Esposito, Steven T., "Applications and Analysis of Raman Lidar Techniques for Measurements of Ozone and Water Vapor in the Troposphere," Master of Science Thesis for Penn State University, Department of Electrical Engineering, May, 1999.

Haris, P.A.T., "Pure Rotational Raman Lidar for Temperature Measurements in the Lower Troposphere," Ph.D. Dissertation, The Pennsylvania State University, 1995.

Holton, J. R., "The Diurnal Boundary Layer Wind Oscillation Above Sloping Terrain," Tellus, 19, 199 – 205, 1967.

Holton, J.R., An Introduction to Dynamic Meteorology, Academic Press, New York, 1972.

Hoxit, L. R., "Diurnal Variations in Planetary Boundary-Layer Winds over Land," Boundary Layer Meteorology, 8, 21 – 38, 1975.

Jenness, J.R., D.B. Lysak, Jr., and C.R. Philbrick, "Design of a Lidar Receiver with Fiber-Optic Output," Applied Optics, 36, No. 18, 4278 – 4284, 1997.

Kobayashi, Takao, "Techniques for Laser Remote Sensing of the Environment," Remote Sensing Reviews, 3, 1 – 56, 1987.

Measures, Raymond M., Laser Remote Sensing.Wiley-Interscience, New York, 1984.

Melfi, S. H., J. D. Lawrence Jr., and M. P. McCormick, "Observation of Raman Scattering by Water Vapor in the Atmosphere," Appl. Phys. Lett., 15, 295 – 297, 1969.

Mulik, K.R., G. Li, G.S. Chadha, and C.R. Philbrick, "Evolution of Air Pollution Events Determined from Raman Lidar," Proceedings of the A&WMA Specialty Conference and Exhibition, PM2000: Particulate Matter and Health, Charleston, South Carolina, 4ASP2: 11-13, January 24-28, 2000.

Mulik, Karoline R., "Evolution of Ozone and Particulate Matter During Pollution Events Using Raman Lidar," Master of Science Thesis for Penn State University, Department of Electrical Engineering, May, 2000.

O'Brien, M.D., T.D. Stevens, and C.R. Philbrick, "Optical Extinction from Raman Lidar Measurements," Optical Instruments for Weather Forecasting, SPIE Proceedings Vol. 2832, 45-52, 1996.

Philbrick, C.R., "Raman Lidar Measurements of Atmospheric Properties," Atmospheric Propagation and Remote Sensing III, SPIE Vol. 2222, 922-931, 1994.

Philbrick, C. Russell, "Investigations of Factors Determining the Occurrence of Ozone and Fine Particles in Northeastern USA," Measurement of Toxic and Related Air Pollutants - Specialty Conference Cosponsored by the Air and Waste Management Association and the U.S. EPA's National Exposure Research Lab, 1, 248-260, 1998.

Philbrick, C. Russell, "Raman Lidar Capability to Measure Tropospheric Properties," Nineteenth International Laser Radar Conference, NASA Langley Research Center, Hampton, VA, NASA Conf. Publ. 207671, 289- 292, July, 1998.

Philbrick, C.R., "Overview of Raman Lidar Techniques of for Air Pollution Measurements," Lidar Remote Sensing for Industry and Environment Monitoring II, SPIE Vol. 4484, 136 - 150, 2001.

Pitchford, K. L., and J. London, "The Low-Level Jet as Related to Nocturnal Thunderstorms Over Midwest United States," J. Appl. Meteor., 1, 43-47, 1962.

Radian International, LAP-3000 Operation and Maintenance Manual, 1999.

Reitebuch, O., A. Strassburger, S. Emeis, W. Kuttler, "Nocturnal Secondary Ozone Concentration Maxima Analysed By Sodar Observations and Surface Measurement," Atmospheric Environment, 34, 4315-4329, 2000.

Ryan, William F., C. R. Philbrick, R. D. Clark, "Meteorological Aspects of the July 15-20, 1999 Northeast Oxidant and Particulate Study (NEOPS) Pollution Episode," 4th Conf. On Atmos. Chem., Amer. Meteor. Soc., 2001.

Ryan, William F., C. R. Philbrick, R. D. Clark, "Summary of Meteorological Conditions During the Northeast Oxidant and Particulate Study (NEOPS) July 2002 Intensive Observing Period," 5th Conf. On Atmos. Chem., Amer. Meteor. Soc., 2003.

Seaman, N. L., and S. A. Michelson , "Mesoscale Meteorological Structure of a High Ozone Period during the 1995 NARSTO Northeast Study," J. Appl. Meteor., 39, 384-398, 1998.

Slick, C.T., "Lower Tropospheric Temperature Measurement Scheme for an Advanced Lidar Atmospheric Profiling System," Master of Science Thesis for Penn State University, Department of Electrical Engineering, May, 2002.

Stensrud, David J., "Importance of Low-Level Jets to Climate: A Review," Journal of Climate, 9, 1698 – 1711, 1996.

Stull, R. B., An Introduction to Boundary Layer Meteorology, Kluwer Academic Publishers, Dordrecht, The Netherlands, 1997.

Willitsford, Adam, P. Jason Collier, Sameer Unni, Sachin J. Verghese, C. Russell Philbrick, Dennis O'Donnell, Eric Hohman, Dale Unruh, Richard Walker,

and Richard Clark, "Development of an Air Pollution Episode During the NEOPS-DEP 2002 Investigation," 5th Conf. On Atmos. Chem., Amer. Meteor. Soc., 2003.

Wolff, G. T., P. J. Lioy, G. D. Wight, R. E. Meyers, and R. T. Cederwell, " An Investigation of Long-Range Transport of Ozone Across the Midwest and Eastern United States," Atmos. Environ., 11, 797 – 802.

Zhang, Kesu, Huiting Mao, Kevin Civeralo, Stephen Berman, Jia-Yeong Ku, S. Trivikrama Rao, Bruce Doddridge, C. Russell Philbrick, and Richard Clark, "Numerical Investigation of Boundary-Layer Evolution and Nocturnal Low-Level Jets: Local versus Non-Local PBL Schemes," Environ. Fluid Mech., 1, 171 – 208, 2001.